BIAXIAL STRENGTH TESTS ON BERYLLIUM AND TITANIUM ALLOYS

U. S. Lindholm, et al

Southwest Research Institute

Prepared for:

Air Force Materials Laboratory

July 1974

Unclassified

SECURITY CLASSIFICATION OF THIS PAGE (When Data Entered)

AD/A002 137

REPORT DOCUMENTATION PAGE		READ INSTRUCTIONS BEFORE COMPLETING FORM
1. REPORT NUMBER AFML-TR-74-172	2. GOVT ACCESSION NO.	3. RECIPIENT'S CATALOG NUMBER
4. TITLE (and Subtitle) BIAXIAL STRENGTH TESTS ON BERYLLIUM AND TITANIUM ALLOYS		5. TYPE OF REPORT & PERIOD COVERED Final July '71 - April '74 6. PERFORMING ORG. REPORT NUMBER 02-3119
7. AUTHOR(s) U. S. LINDHOLM L. M. YEAKLEY D. L. DAVIDSON		8. CONTRACT OR GRANT NUMBER(s) F33615-71-C-1608
9. PERFORMING ORGANIZATION NAME AND ADDRESS SOUTHWEST RESEARCH INSTITUTE DEPARTMENT OF MATERIALS SCIENCES P. O. DRAWER 28510, SAN ANTONIO, TX. 78284		10. PROGRAM ELEMENT, PROJECT, TASK AREA & WORK UNIT NUMBERS Project No. 7351 Task No. 735106
11. CONTROLLING OFFICE NAME AND ADDRESS AIR FORCE SYSTEMS COMMAND Aeronautical Systems Div., 4950/PMRA Wright-Patterson Air Force Base, Ohio 45433		12. REPORT DATE July 1974 13. NUMBER OF PAGES<br~~55~~ 56
14. MONITORING AGENCY NAME & ADDRESS (if different from Controlling Office) Air Force Materials Laboratory (LLN) Wright-Patterson AFB, Ohio 45433		15. SECURITY CLASS. (of this report) UNCLASSIFIED 15a. DECLASSIFICATION/DOWNGRADING SCHEDULE

16. DISTRIBUTION STATEMENT (of this Report)

Approved for public release; distribution unlimited.

17. DISTRIBUTION STATEMENT (of the abstract entered in Block 20, if different from Report)

18. SUPPLEMENTARY NOTES

19. KEY WORDS (Continue on reverse side if necessary and identify by block number)

BERYLLIUM
TITANIUM
BIAXIAL STRENGTH
YIELD
PLASTIC FLOW
FAILURE
PRESTRAINING

20. ABSTRACT (Continue on reverse side if necessary and identify by block number)

Results of extensive biaxial testing of two new grades of beryllium and two titanium alloys, 6Al-4V and 6Al-6V-2Sn, are presented. The tests are conducted on thin walled tubular specimens subject to combinations of axial load, torsion and internal pressure. The results include description of the yield, plastic flow and failure properties of these alloys under plane stress conditions. In each case, yield and plastic flow is adequately

DD FORM 1473 EDITION OF NOV 65 IS OBSOLETE

Unclassified (56)

SECURITY CLASSIFICATION OF THIS PAGE (When Data Entered)

described by a Mises yield criterion and associated flow rule. Tensile failure is more accurately described by a maximum stress criterion, particularly for the beryllium which has low ductility. Biaxial ductility is shown to be very sensitive to both the form of the failure stress criterion and to the strain hardening modulus of the material. The effect of prestraining on subsequent ductility in beryllium is examined.

NOTICE

When Government drawings, specifications, or other data are used for any purpose other than in connection with a definitely related Government procurement operation, the United States Government thereby incurs no responsibility nor any obligation whatsoever; and the fact that the government may have formulated, furnished, or in any way supplied the said drawings, specifications, or other data, is not to be regarded by implication or otherwise as in any manner licensing the holder or any other person or corporation, or conveying any rights or permission to manufacture, use, or sell any patented invention that may in any way be related thereto.

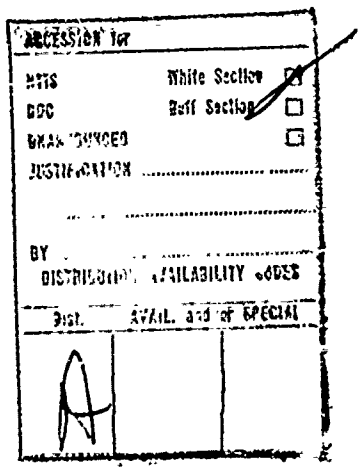

Copies of this report should not be returned unless return is required by security considerations, contractual obligations, or notice on a specific document.

FOREWORD

This report was prepared by the Department of Materials Sciences, Southwest Research Institute, San Antonio, Texas under USAF Contract No. F33615-71-C-1608. The contract was initiated under Project No. 7351, "Metallic Materials," Task No. 735106, "Behavior of Metals." The work was monitored by the Metals Behavior Branch, Metals and Ceramics Division, Air Force Materials Laboratory with Mr. M.J. Sever (AFML/LLN) acting as project scientist.

This work was supported, in part, by funds provided by Defense Nuclear Agency under Subtask N99QAXAA110, "ABM Vulnerability Studies" Work Unit II, "Beryllium Substructure Evaluation."

This report covers work conducted from July 1971 to April 1974.

The report was submitted by the authors in July 1974.

This technical report has been reviewed and is approved.

G.R. ATKINS
Project Engineer

FOR THE COMMAND

V.J. RUSSO
Actg Chief, Metals Behavior Branch
Metals and Ceramics Division
Air Force Materials Laboratory

Copies of this report should not be returned unless return is required by security considerations, contractual obligations, or notice on a specific document.

TABLE OF CONTENTS

ILLUSTRATIONS

ILLUSTRATIONS (Cont'd.)

TABLES

SECTION I

INTRODUCTION

A previous study by the authors [Reference 1] determined the effects of strain rate, temperature and biaxial stress states on the strength and ductility of S-200E beryllium and titanium 6Al-4V. The present report is concerned primarily with the biaxial strength properties of two newer grades of beryllium and two titanium alloys, 6Al-4V and 6Al-6V-2Sn. The test specimens are thin-walled machined tubes. All tests were performed on a servo-controlled, hydraulic biaxial testing machine which is described in Reference 2. The tubes were subjected to combinations of axial, torsional, and internal pressure loading to produce a range of plane stress conditions. Testing was conducted to failure along both proportional and nonproportional load paths.

The previous biaxial tests [Reference 1] demonstrated the strong dependence of ductility, as measured by the effective strain at failure, on the state of stress for both beryllium and titanium. Ductility was shown to be reduced significantly under biaxial tensile stresses. Jortner [Reference 3] subsequently found similar behavior in tests of HP-21 grade beryllium hot pressed block. Jortner showed that the biaxial failure strain behavior could be accounted for by imposing a maximum stress failure criteria upon deformation described by a Mises type quadratic flow rule. It was also shown that the extent of biaxial ductility reduction is strongly dependent upon the strain hardening coefficient.

Another factor which has been of concern relative to the ductility of beryllium is the potentially adverse effect of precompression [References 3 and 4]. Some tests have indicated that precompression may tend to exhaust ductility and lead to brittle behavior on subsequent tensile loading. The present work explores the effect of both precompression and pretorsion on the subsequent strain hardening and ductility when the specimen is reloaded in other stress directions, including reversed loading.

After describing the general test procedures in the next section, the test results and discussions are presented in separate sections on beryllium and titanium.

SECTION II

TEST PROCEDURES

All tests described were performed on a biaxial test facility previously developed for AFML. This facility is described in Reference 2 and is shown in Figure 1. It is a servo-controlled, hydraulic machine with two independent feedback loops. The hydraulic actuator (mounted below the lower platten in Figure 1) in this machine produces combined axial and torsional load or displacement. Each component is independently controlled from either load, displacement or strain transducers. This configuration of the machine provides for combined axial compression/tension and torsion testing. In addition, programable internal pressure within a tubular specimen is supplied by a separate servo-controlled pressure intensifier (not shown). This mode provides for variable circumferential hoop tension in the specimen. Only two of the three available loading modes have been exercised at one time. Thus, the test data are obtained with either combined axial compression/tension and torsion or with axial compression/tension and internal pressure (hoop tension). The load capacities of the test facility are ±10,000 lb axial load, ±3000 in-lbs torque, and 20,000 psi internal pressure.

The applied loading is measured with a strain gage type biaxial (axial/torsional) load cell or a pressure cell located on the high pressure side of the pressure intensifier.

Strains are measured within the uniform gage section of the specimen using two types of biaxial extensometer [Reference 1]. The axial/torsional extensometer is of the capacitance type. Strain gaged flexural clip type extensometers are used for the combined axial and hoop strain measurements. These extensometers have sufficient dynamic range to measure both the elastic and plastic components of strain to failure of the specimen. Bonded resistance strain gages were used in a few cases to supplement and to verify the extensometer measurements.

The stresses and strains reported are average sectional values and are based upon a small strain measure. The data presented are engineering stress and strain values. Finite deformation corrections are small within the range of failure strains for beryllium and within the strain hardening region for titanium. Failure in titanium may occur after considerable plastic flow beyond the point of maximum load. The failure strains reported under these conditions should be compared with percent

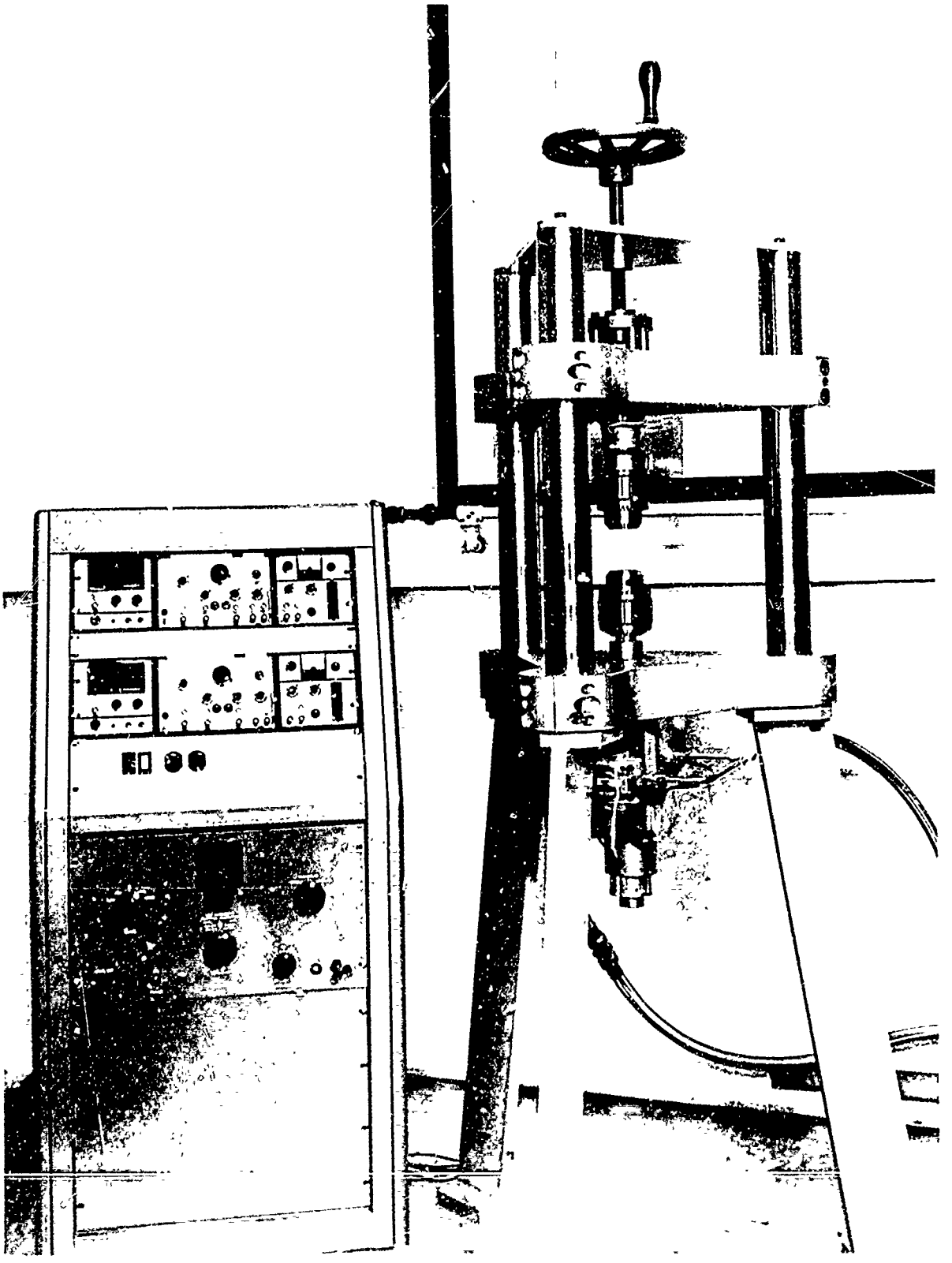

Figure 1. Biaxial Testing Machine

elongation measurements in uniaxial tensile tests. At this point the deformation is large and the strain is no longer uniformly distributed over the gage length.

Since both stress (load) or strain (deformation) can be used as a feedback control signal on both axes of a biaxial test, some choice is available for the two independent control functions. In the present testing, it was decided to control strain rate on one axis and control stress ratio on the second axis. Since strain rate is controlled on one axis only, there is some small variation during plastic straining of the total effective strain rate which was held at approximately 10^{-3} sec^{-1} for all tests. The stress ratio control provided for proportional loading paths. The nonproportional paths, referred to earlier, are actually piecewise proportional; i.e., initial loading and unloading along one proportional path (e.g., uniaxial compression) followed by a second loading to failure with a different constant stress ratio.

The dimensions of the test specimens are given in Figure 2. The beryllium specimens were chemically etched in the gage section after machining in order to remove any potential surface damage.

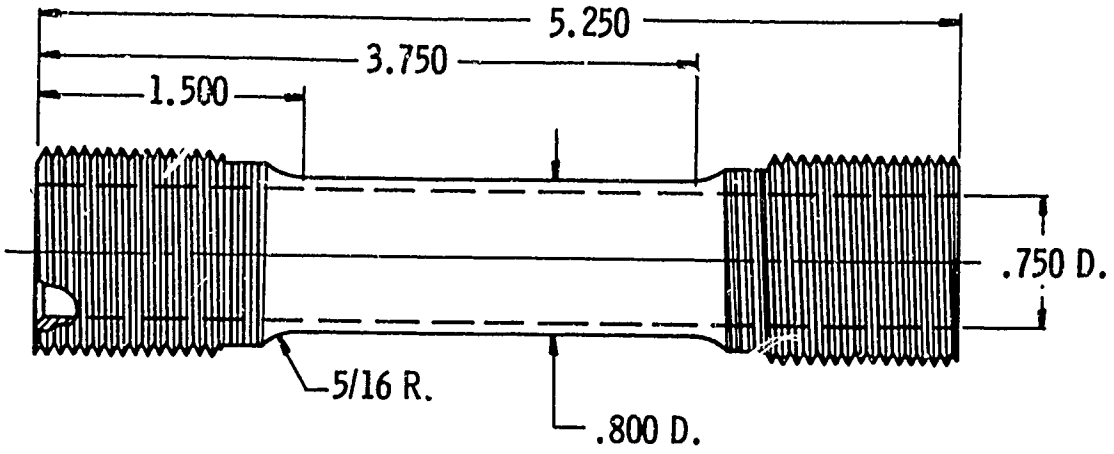

a. Beryllium Specimens

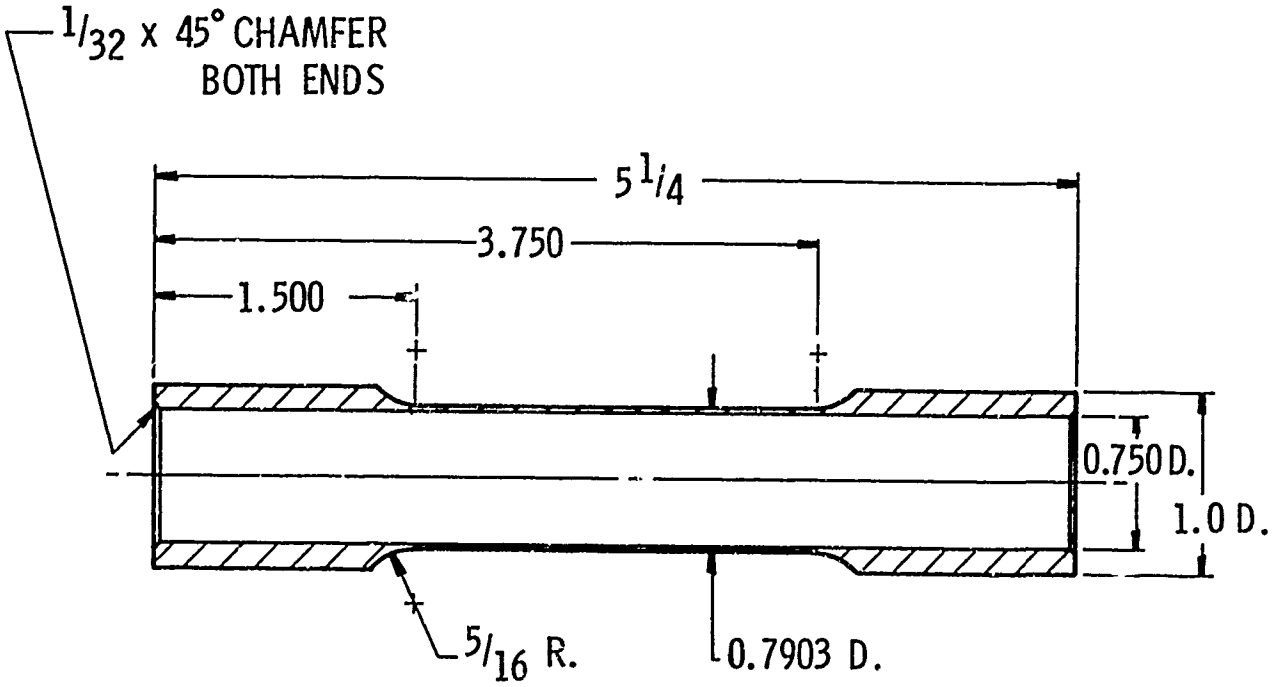

b. Titanium Specimens

Figure 2. Beryllium and Titanium Test Specimens

SECTION III

BERYLLIUM

A. MATERIALS

The beryllium specimens were machined from material fabricated by two different processes, both using advanced powders. The material designated XN50C* was formed as hot-pressed block and was supplied by Brush-Wellman, Inc. The second material, supplied by Kawecki Berylco Industries (KBI), was consolidated from high purity KBI P1 powder by the process of cold isostatic pressing followed by hot isostatic pressing (CIP/HIP).

The specimens were machined and surface etched by the Speed Ring Corporation and subsequently radiographed at AFML.

B. BIAXIAL STRENGTH AND DUCTILITY

The biaxial strength data will be presented in the form of selected effective stress-strain curves to illustrate strain hardening behavior and two dimensional plots of yield and failure stresses and strains to failure. The data are also summarized in Tables I and II.

The data are presented in terms of the normal stresses, σ_L and σ_T, and the shear stress σ_{LT}. The corresponding strains are ϵ_L, ϵ_T and ϵ_{LT}. The subscripts L and T refer to the longitudinal and transverse directions in the tubular specimens, longitudinal being in the direction of the tube axis. The stress-strain curves are given in terms of "effective" stress and strain defined by

$$\sigma_{eff} = \left[\sigma_L^2 - \sigma_L \sigma_T + \sigma_T^2 + 3\sigma_{LT}^2\right]^{1/2} \quad (1)$$

and

$$\epsilon_{eff} = \left[\epsilon_L^2 + \epsilon_L \epsilon_T + \epsilon_T^2 + 1/3\, \epsilon_{LT}^2\right]^{1/2} \quad (2)$$

Equation 2 incorporates the assumption of incompressibility and thus is only approximate when total strains are plotted.

---

*Currently designated as S-65 grade.

TABLE I. DATA SUMMARY - BERYLLIUM XN50C

Specimen No.	0.2% Yield Strength (KSI)				Ult. Strength (KSI)			Strain at Fracture (%)		
	σ_L	σ_{LT}	σ_T	$\bar{Y}_o$	σ_L	σ_{LT}	σ_T	ϵ_L	ϵ_{LT}	ϵ_T
B- 2	34.0	0		34.0	44.0	0		2.38	N.R.	
3	0	17.0		29.4	0	35.0		N.R.	9.30	
4	17.3	16.0		32.6	28.7	26.1		2.41	6. 9	
6	24.6	13.0		33.4	37.9	18.7		2.48	3.58	
7	0	18.0		31.2	0	34.0		0.31	6.82	
8	9.3	18.5		33.4	16.4	33.0		1.48	7.86	
9	-36.6	0		36.6	-50.0	N.R.		-4.3	N.R.	
10	0		29.0	29.0	0		48.7	-1.59		4.02
12	29.1		30.2	29.7	44.7		46.6	1.35		1.1
13	33.1		17.5	28.7	45.3		24.1	1.52		0
14	17.1		35.9	31.1	24.4		51.35	0		2.00
15	31.8		0	31.8	46.0		0	2.55		-1.08
16	-34.1		0	34.7	-64.3		0	-3.74		1.94
18	-23.7		11.7	31.3	-46.8		23.5	-4.46		3.23
19	-18.3		18.4	31.7	-36.5		36.2	-4.58		4.2
20	-11.4		23.4	30.8	-21.6		44.0	-4.46		6.13
22	30.0		0	29.9	45.1		0	2.29		-0.99
23*	-31.4		0	31.4	47.6		0	2.88		-1.31
27*	-30.2		0	30.2	49.5		0	-1.01		3.10
28*	-31.5		0	31.5	-37.2		36.5	-4.45		3.73
29*	-28.0		0	28.0	48.6		48.1	1.53		1.20
30	0		28.3	28.3	0		48.6	-1.50		3.62
31	8.7		35.1	31.6	12.3		49.7	-0.56		2.85
32	24.5		35.7	31.6	34.9		48.6	0.56		1.71
33	32.6		31.1	31.9	48.1		47.1	1.44		1.03
35	33.2		23.1	29.5	47.2		33.6	1.39		0.24
36	32.6		8.3	29.3	45.2		11.5	1.52		-0.31

TABLE I. DATA SUMMARY - BERYLLIUM XN50C (Cont'd.)

Specimen No.	0.2% Yield Strength (KSI)				Ult. Strength (KSI)			Strain at Fracture (%)		
	σ_L	σ_{LT}	σ_T	$\bar{Y}_o$	σ_L	σ_{LT}	σ_T	ϵ_L	ϵ_{LT}	ϵ_T
B- 37	27.8		30.9	29.4	44.3		46.6	1.59		1.61
40*	28.1		32.1	30.3	44.4		47.2	1.61		1.54
41*	-31.3		0	31.3	0	34.2		0.36	7.94	
42	0	22.4		38.7	0	28.0		N.R.	8.76	
43**	-32.8		0	32.8	0		54.1	-2.96		3.65
44*	-30.4			30.4	0	33.2		0.19	7.18	
46	-33.1		0	33.1	No failure		0			
47**	-34.5			34.5	29.1	28.7		1.84	4.32	
48**	-33.6			33.6	0	35.9		0.05	5.57	
49**	-31.1			31.1	53.9		0	-0.49		0.28
50**	-29.4			29.4	49.0		51.4	-1.51		1.53
52**	-30.9			30.9	27.7		57.4	-2.02		1.89
53	30.0	0		30.0	43.0	0		2.55	N.R.	
55	-31.5		0	31.5	-36.5		35.4	-3.93		3.20
56		15.3		26.5	49.2		50.1	0.91		0.67
58***		17.2		29.9	0		48.7	-0.85		2.15
59***		17.3		30.0	26.6	28.6		2.82	5.74	
60***		18.2		31.5	-33.0		33.8	-3.71		2.50
61***		20.4		35.4	0	33.7		0.74	8.76	
62***				25.9	45.4		0	1.55		-0.54

Nonproportional Loading Paths
* 1% Comp. Prestrain
** 2.5% Comp. Prestrain
*** 2.5% Torsional Prestrain

TABLE II. DATA SUMMARY - BERYLLIUM P1

Specimen No.	0.2% Yield Strength (KSI) σ_L	σ_{LT}	σ_T	$\bar{Y}_o$	Ult. Strength (KSI) σ_L	σ_{LT}	σ_T	Strain at Fracture (%) ϵ_L	ϵ_{LT}	ϵ_T
K- 3*	-43.0			43.0	-77.0			-3.90		2.10
5*	-43.7			43.7	-44.53		45.2	-4.06		3.45
6**	-44.2			44.2		43.5		0.27	5.12	
7*	-42.2			42.2		46.0		0.15	6.77	
8*	-42.8			42.8	36.2	34.2		2.51	6.20	
10	40.0			40.0	61.0			2.38		
11	12.0	21.7		39.6	21.5	40.5		1.52	8.30	
12***		24.3		42.1	- 1.0		59.2	-0.44		1.10
15	31.6	12.7		38.8	48.8	23.2		2.32	3.23	
16										
17**	-42.0			42.0	32.9	30.8		0.85	1.42	
18										
19*	-40.5			40.5	60.5		62.8	0.46		1.15
20*	-42.4			42.4	63.6			1.87		-0.75
21										
22*	-43.5			43.5	57.4			0.98		-0.46
23										
24**	-41.0			41.0	65.8			0.70		-0.31
25*	-41.7			41.7			59.4	-1.27		2.07
27	42.9		42.4	42.7	62.3		62.6	1.40		1.30
28*	-40.5			40.5			63.4	-1.67		2.72
29***		25.4		44.0	64.9			2.17		-0.98
30**	-38.6			38.6	58.2		67.3	-0.98		1.74
31	48.2		32.4	42.6	53.1		44.6	1.11		0.23
33***		24.7		42.8	57.1		64.6	0.79		0.79
34	-31.6		15.5	41.5	-57.2		28.8	-3.59		2.82

TABLE II. DATA SUMMARY - BERYLLIUM P1 (Cont'd.)

Specimen No.	0.2% Yield Strength (KSI)				Ult. Strength (KSI)			Strain at Fracture (%)		
	σ_L	σ_{LT}	σ_T	$\bar{Y}_o$	σ_L	σ_{LT}	σ_T	ϵ_L	ϵ_{LT}	ϵ_T
K- 35	11.9		46.3	41.6	14.4		64.4	-0.31		1.13
36	-43.7			43.7	-77.9			-3.30		1.54
37**	40.1			40.1			67.7	-2.56		3.65
38**	-39.0			39.0	-44.5		44.6	-4.15		3.38
39	-21.9		21.6	37.7	-42.9		42.3	-3.58		3.52
40	-45.4			45.4	-80.5			-3.22		1.54
41	-15.2		31.4	41.2	-26.6		53.8	-3.01		4.18
42	46.4		22.9	40.2	61.9		29.0	0.89		0.03
43	33.7		48.0	42.7	48.3		66.0	0.56		1.27
44***		25.4		44.0	-45.7		48.6	-3.55		3.32
45***		23.2		40.2		-46.0		0.19	-6.83	
46			42.9	42.9			61.4	-0.80		1.85
49	37.2		37.5	37.4	60.8		63.9	1.47		1.41
50		22.4		38.8		46.5			8.67	
51	22.3	21.2		43.0	36.6	36.1		2.09	5.73	
52	42.9			42.9	63.4			2.33		-1.03
53	23.7		49.5	42.9	32.1		67.8	0.05		1.55
56	49.9		39.0	45.5	63.9		49.7	0.96		0.49
57	46.6		57.9	53.2	63.7		56.9	1.17		0.90
58	44.2		40.2	42.4	60.5		61.7	0.91		1.16
59	41.6		45.4	43.6	58.5		62.2	0.72		1.23
60	33.9		43.3	39.5	46.5		62.4	0.34		1.20

Nonproportional Loading Paths
* 1% Comp. Prestrain
** 2.5% Comp. Prestrain
*** 2.5% Torsional Prestrain

For the materials tested, the yield condition is closely approximated by the condition

$$\sigma_{eff} = \bar{Y}_o \tag{3}$$

where $\bar{Y}_o$ is a constant. This is equivalent to a Mises yield criterion with $\bar{Y}_o$ being the yield strength in simple tension. The effective stress and strain definitions result from integration of the associated flow rule for proportional loading. A check of the experimental plastic strain increments showed normality to the Mises yield ellipse, Equation 3, for all stress ratios.

Figures 3, 4 and 5 show effective stress-strain curves for the Brush XN50C beryllium. The loading path associated with each curve is shown in the lower right of each figure. The arrows indicate the fracture strain.

Figure 3 shows the uniaxial tensile stress-strain curve (open circles) and several curves for specimens initially loaded to a compressive prestrain of $\epsilon_L = 1\%$, unloaded, and reloaded along the indicated stress path to failure. There are several things to note:

(a) The XN50C beryllium exhibits a distinct yield plateau following initial yield. This yield plateau is eliminated by cold work, not being present on reloading.

(b) Reversed loading, compression followed by tension (triangles), shows a relatively strong Baushinger effect with second yield occurring at a low value of tensile stress.

(c) For reloading in the transverse or biaxial stress directions, the yield point is enhanced. Initial yield occurs at 32 ksi in tension and compression. The compressive prestrain hardens the material to about 40 ksi. This is approximately the yield stress for reloading in the transverse or biaxial directions.

(d) Finally, it is observed that the ductility or strain to failure depends quite strongly on the stress ratio. Examination of Table I will show this for simple proportional loading to failure. The effect of 1% precompression does not in itself reduce ductility. In fact, if ductility is measured by cumulative plastic strain or by total plastic work (area under the effective stress-strain curve) to failure, the precompressed specimens show increased ductility in some cases.

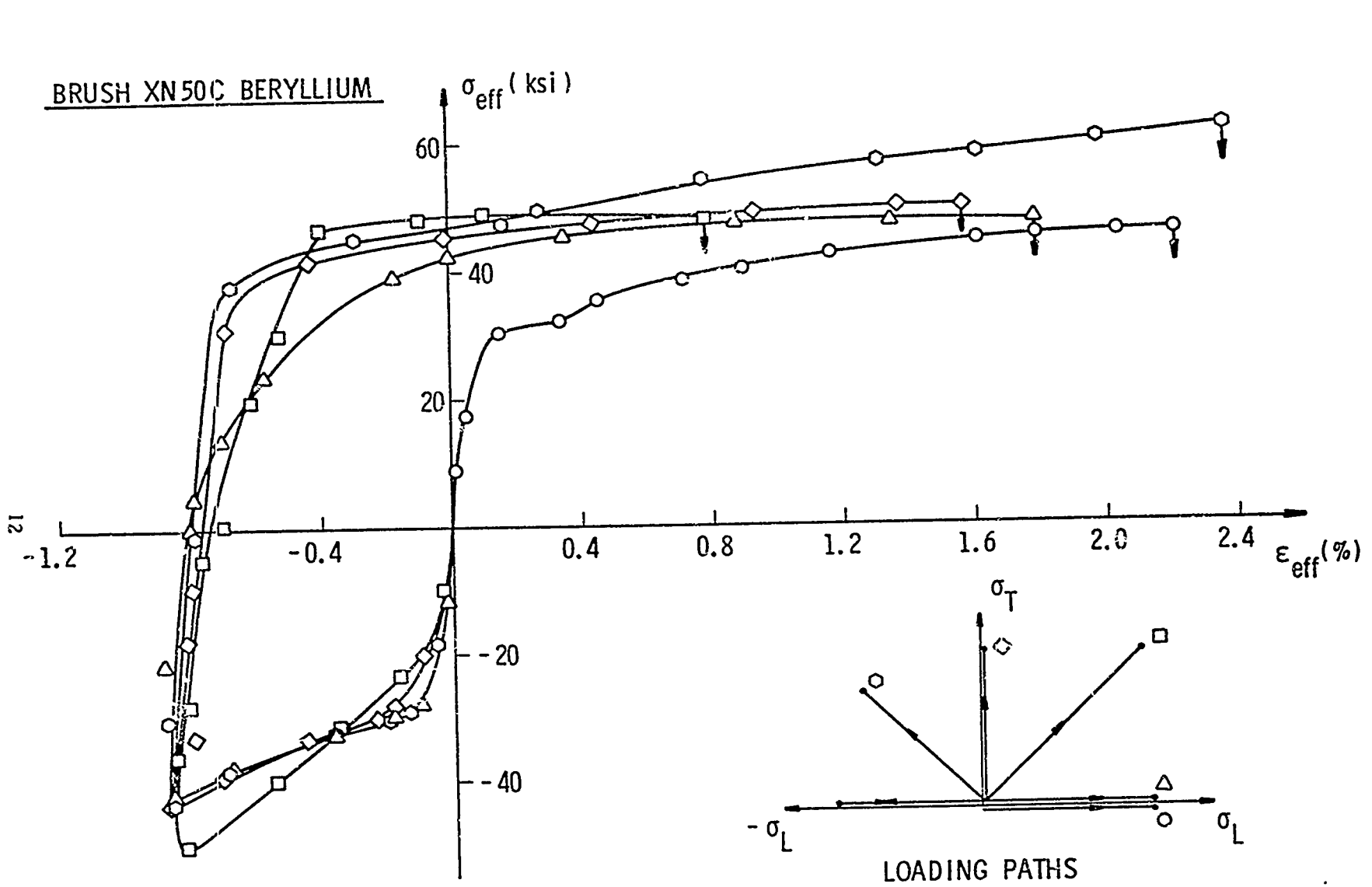

Figure 3. Effective Stress-Strain Curves for Be (XN50C), 1% Axial Compressive Prestrain

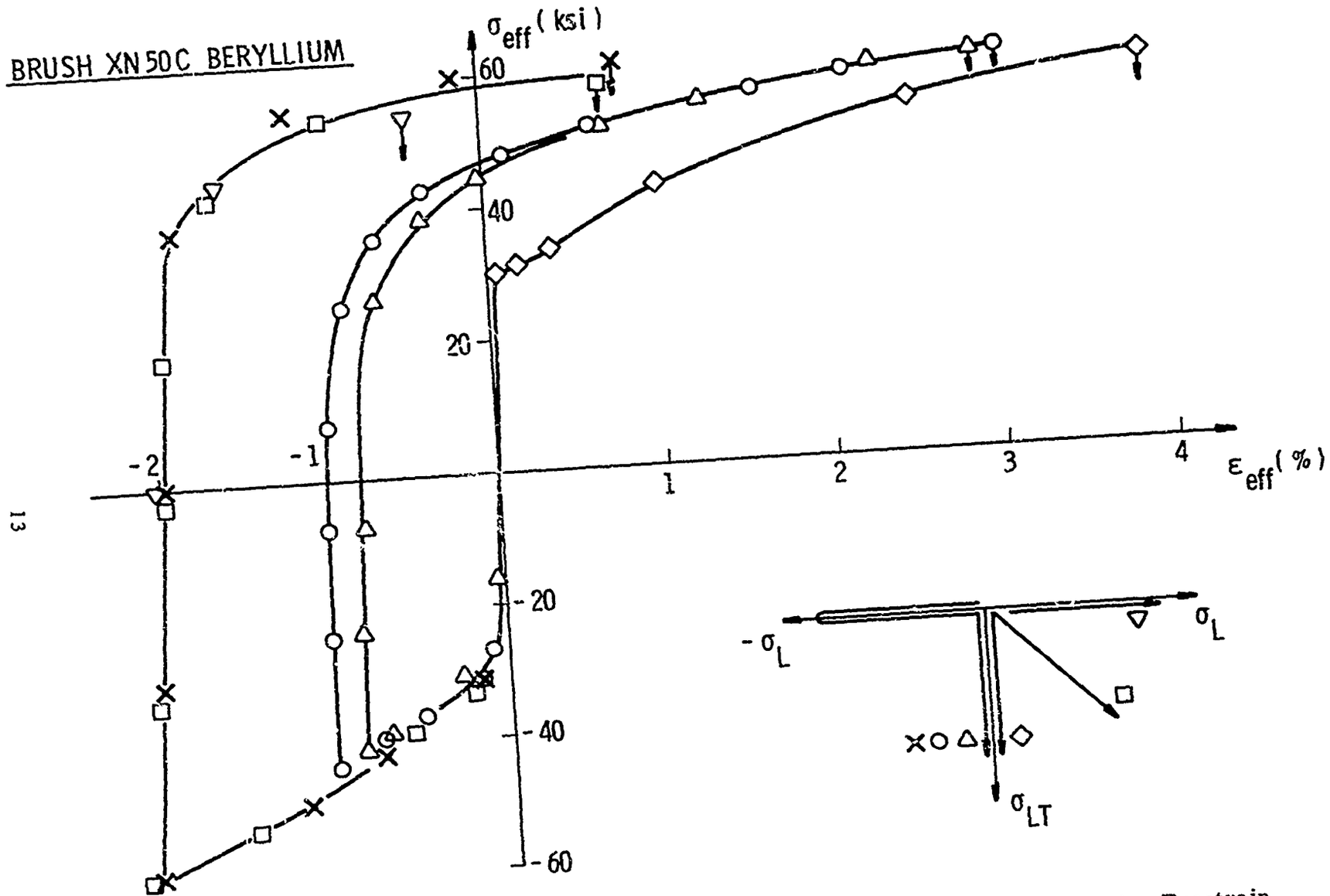

Figure 4. Effective Stress-Strain Curves for Be (XN50C), 1% and 2.5% Axial Compressive Prestrain

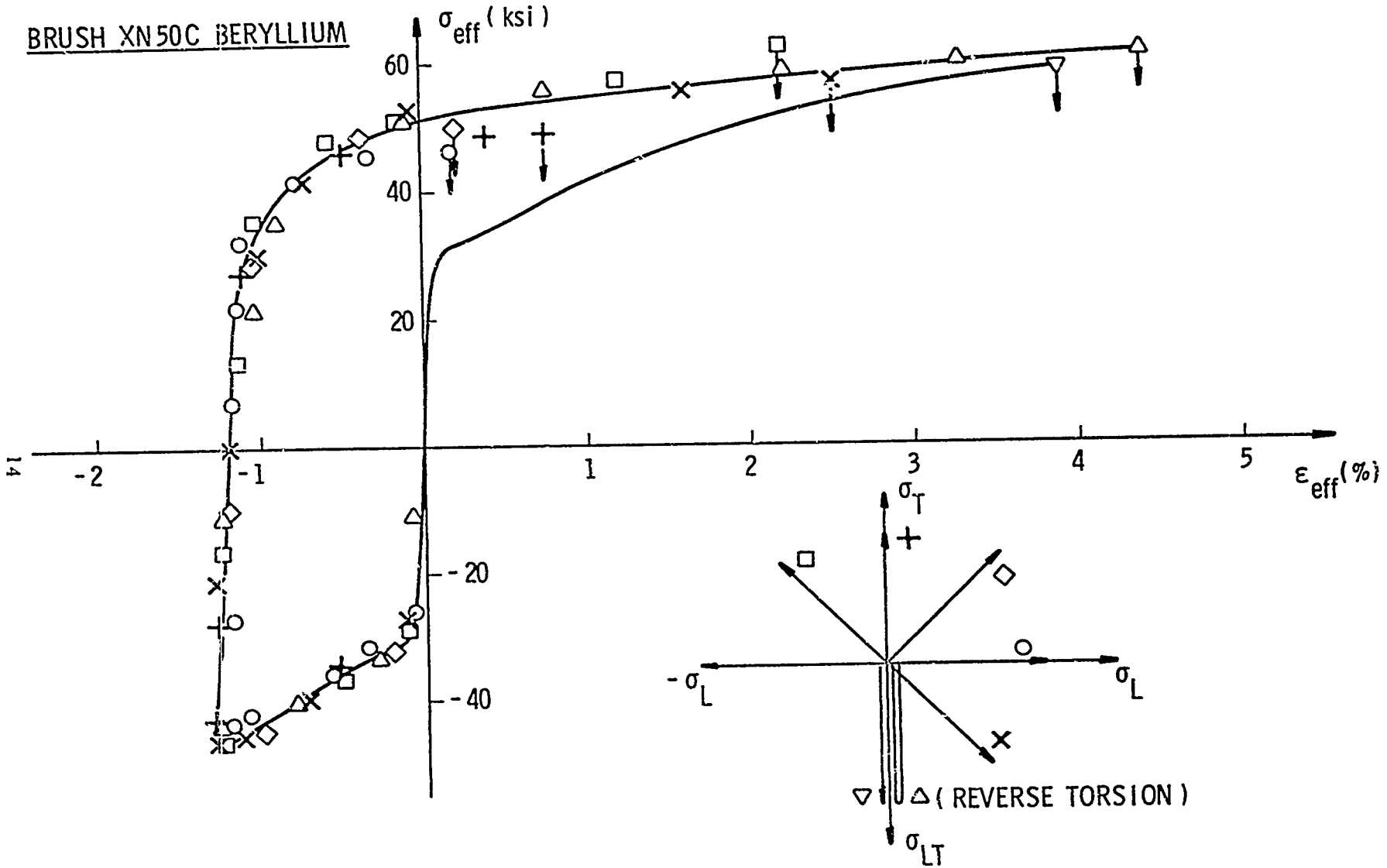

Figure 5. Effective Stress-Strain Curves for Be (XN50C), 2.5% Torsional Prestrain

Figure 4 illustrates precompression followed by torsion and combined torsion and tension. The torsional stress-strain curve is given also. This curve exhibits the same yield plateau on initial loading noted in tension.

Figure 5 shows curves for specimens prestrained in torsion to ϵ_{LT}=2.5%. The many reloading conditions all follow a similar effective stress-strain path. The larger prestrains of 2.5% compression or torsion do suggest some reduction in subsequent ductility, particularly for tensile failures. Reversed torsion shows enhancement of ductility.

The strength data for XN50C beryllium are plotted in Figure 6. The 0.2% yield strength is in good agreement with the Mises ellipse (Equation 3) as shown. The value of Y_o for each test is given in Table I. The average value, based on all 47 tests, is 31.25 ksi with a standard deviation of 2.38 ksi.

Stresses at failure for both the proportional load paths (open data points) and the three different prestrain conditions are shown. The stresses at failure for preloaded and monotonically loaded specimens are nearly the same. Failure for all specimens occurs at a fully work-hardened state.

The equation used to fit the failure data is derived from a criterion proposed by Mogi [Reference 5] for failure in rock. The original form given by Mogi is

$$\tau_{OCT} = f\left[\sigma_m - (1-\alpha)\,\sigma_i\right] \tag{4}$$

where τ_{OCT} is the octahedral shear stress, σ_m is the mean stress, σ_i is the intermediate principal stress and α is a constant. This is a modification of the classical Coulomb-Mohr failure criterion for brittle materials. It includes the effect of the intermediate principal stress which is not included in the Coulomb-Mohr criterion but has been shown experimentally to be important. The effect of the mean stress upon failure is shown by the differential between tensile and compressive failure strength in Figure 6.

Equation 4 may be rewritten in the form

$$A\,\sigma_m + B\,\sigma_{eff}^2 + C\,\sigma_i = 1 \tag{5}$$

where σ_m is the sum of the principal stresses, σ_{eff} is given by Equation 1, and σ_i is the intermediate principal stress. If the constants A, B and C are given in terms of the uniaxial tensile strength σ_t, compressive strength σ_c,

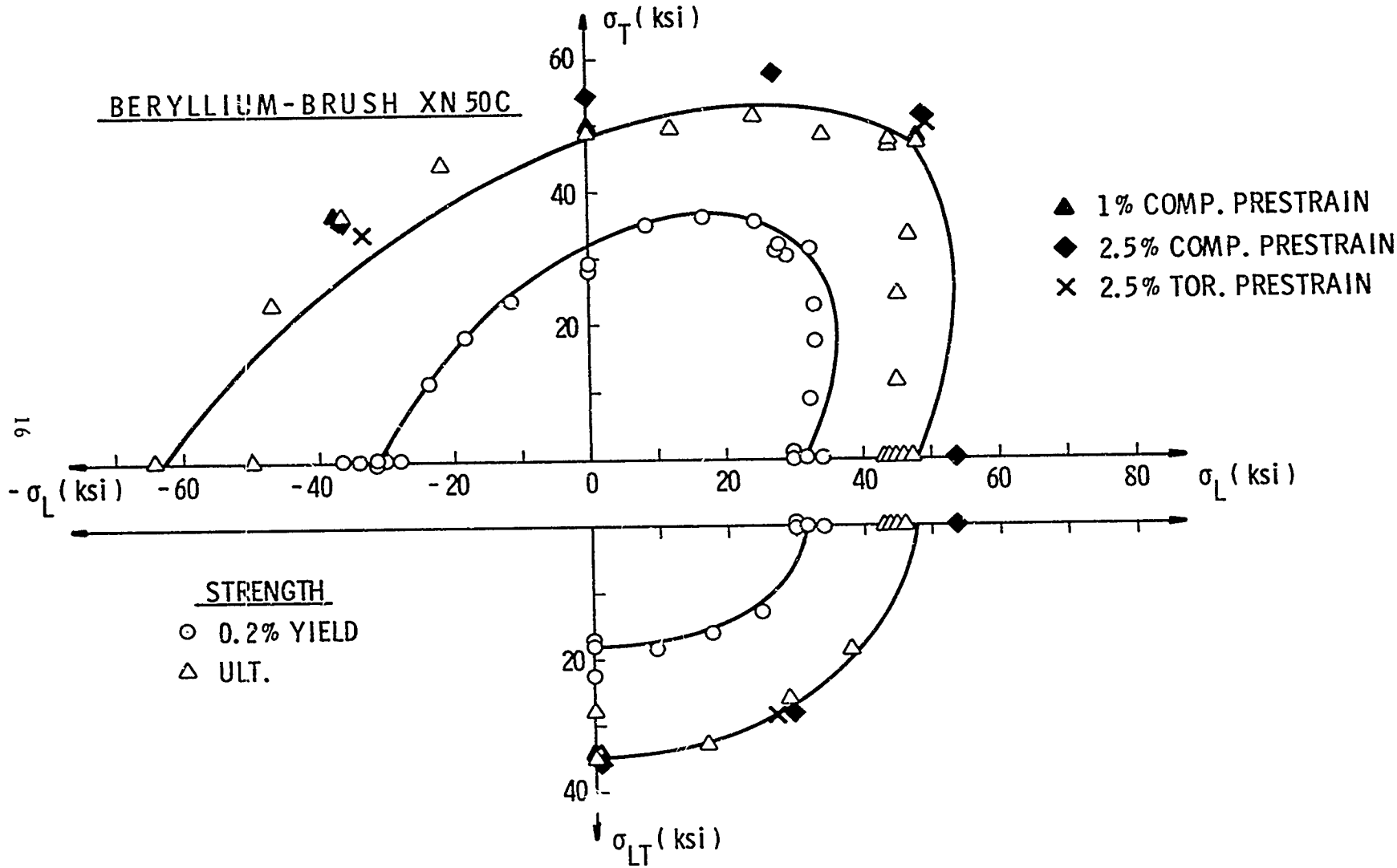

Figure 6. Biaxial Yield and Failure Strengths for Be (XN50C)

and biaxial tensile strength σ_{tt}, then

$$A = \frac{\sigma_t (\sigma_{tt}^2 - \sigma_c^2) + \sigma_{tt} (\sigma_c^2 - \sigma_t^2)}{\sigma_t \sigma_c \sigma_{tt} (\sigma_t - \sigma_c - \sigma_{tt})} \tag{6a}$$

$$B = \frac{\sigma_{tt} (\sigma_c - \sigma_t) - \sigma_t \sigma_c}{\sigma_t \sigma_c \sigma_{tt} (\sigma_t - \sigma_c - \sigma_{tt})} \tag{6b}$$

$$C = \frac{(\sigma_t + \sigma_c) \left[\sigma_t \sigma_c - \sigma_{tt}^2 + 2 \sigma_{tt} (\sigma_t - \sigma_c)\right]}{\sigma_t \sigma_c \sigma_{tt} (\sigma_t - \sigma_c - \sigma_{tt})} \tag{6c}$$

The solid line through the failure data points in Figure 6 is based on Equations 5 and 6 with

$$\sigma_t = 48 \text{ ksi}$$
$$\sigma_c = 63 \text{ ksi}$$
$$\sigma_{tt} = 47 \text{ ksi}$$

A maximum shear stress (Tresca) or normal stress criterion would give a better fit to the data in the tension-tension quadrant, but would not be as satisfactory elsewhere. This will be discussed further in a following section.

The strains measured at failure are plotted in Figure 7. Again the open data points represent monotonic proportional loading to failure and the closed data points are for prestrained specimens. This plot demonstrates the large effect of stress (or strain) ratio on the strain at failure. The shear directions show maximum ductility, while the minimum occurs along the normal strain axes. These minima occur at the stress ratios $\sigma_1 : \sigma_2 = 2:1$. Discussion of the shape of this curve will be given later. The 2.5% compressive prestrain is the most severe from the point of view of plastic work. The failure strains for this condition are shifted strongly in the direction of the precompression, $-\epsilon_L$.

The macroscopic modes of failure are shown in Figure 8 for the entire range of stress ratio. These specimens were all monotonically loaded; however, the prestrained specimens were similar. In compression, the failure is initiated by the circumferential tensile strain producing longitudinal cracks. In pure compression there is a large number of parallel longitudinal cracks formed. This initial fracture is followed by axial buckling of the tube as can be seen in Figure 8 for all compression loaded specimens. The sudden release of internal pressure causes the machine to apply a strong axial load component. There is no evidence that buckling preceded fracture.

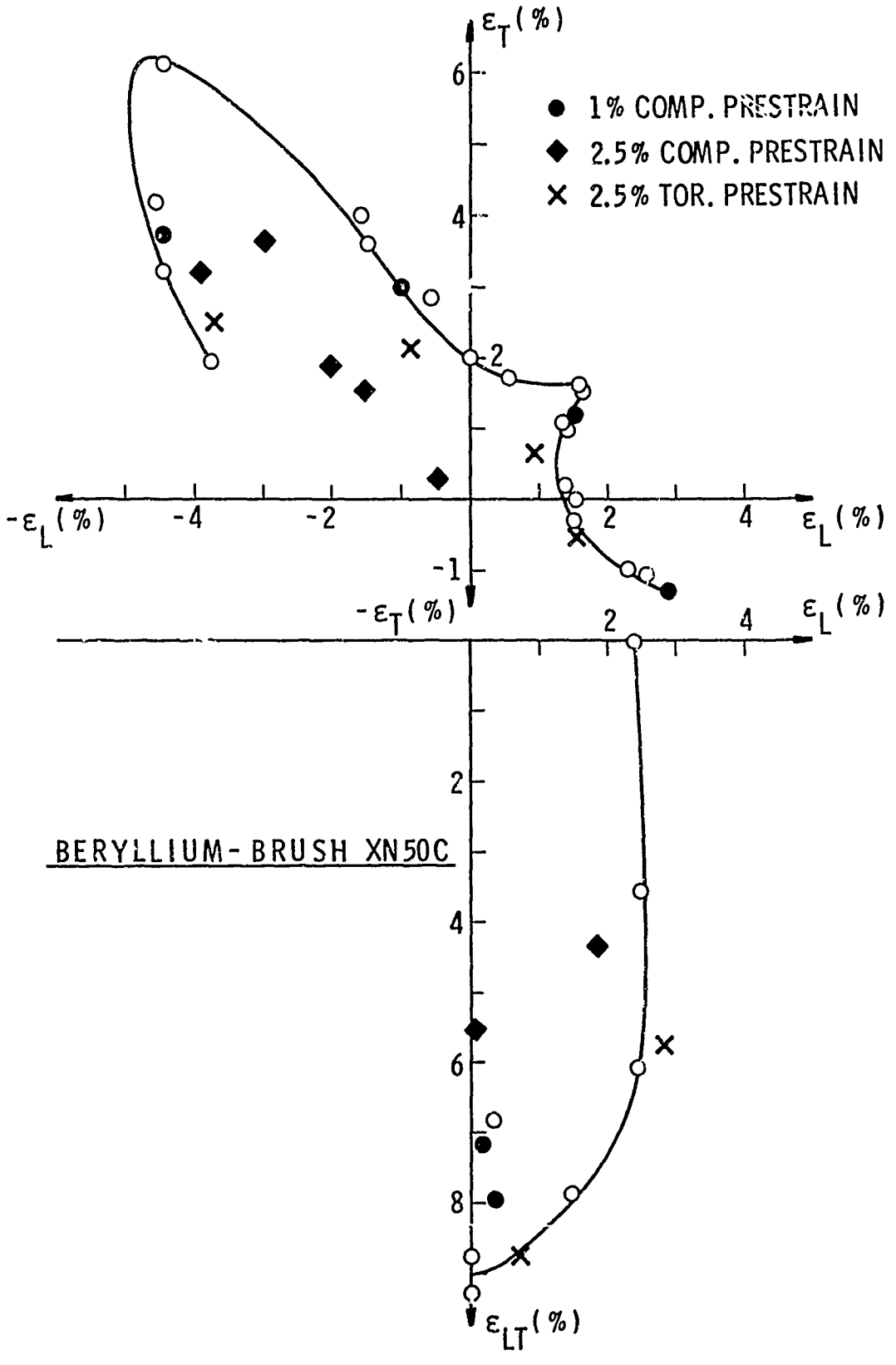

Figure 7. Biaxial Failure Strains for Be (XN50C)

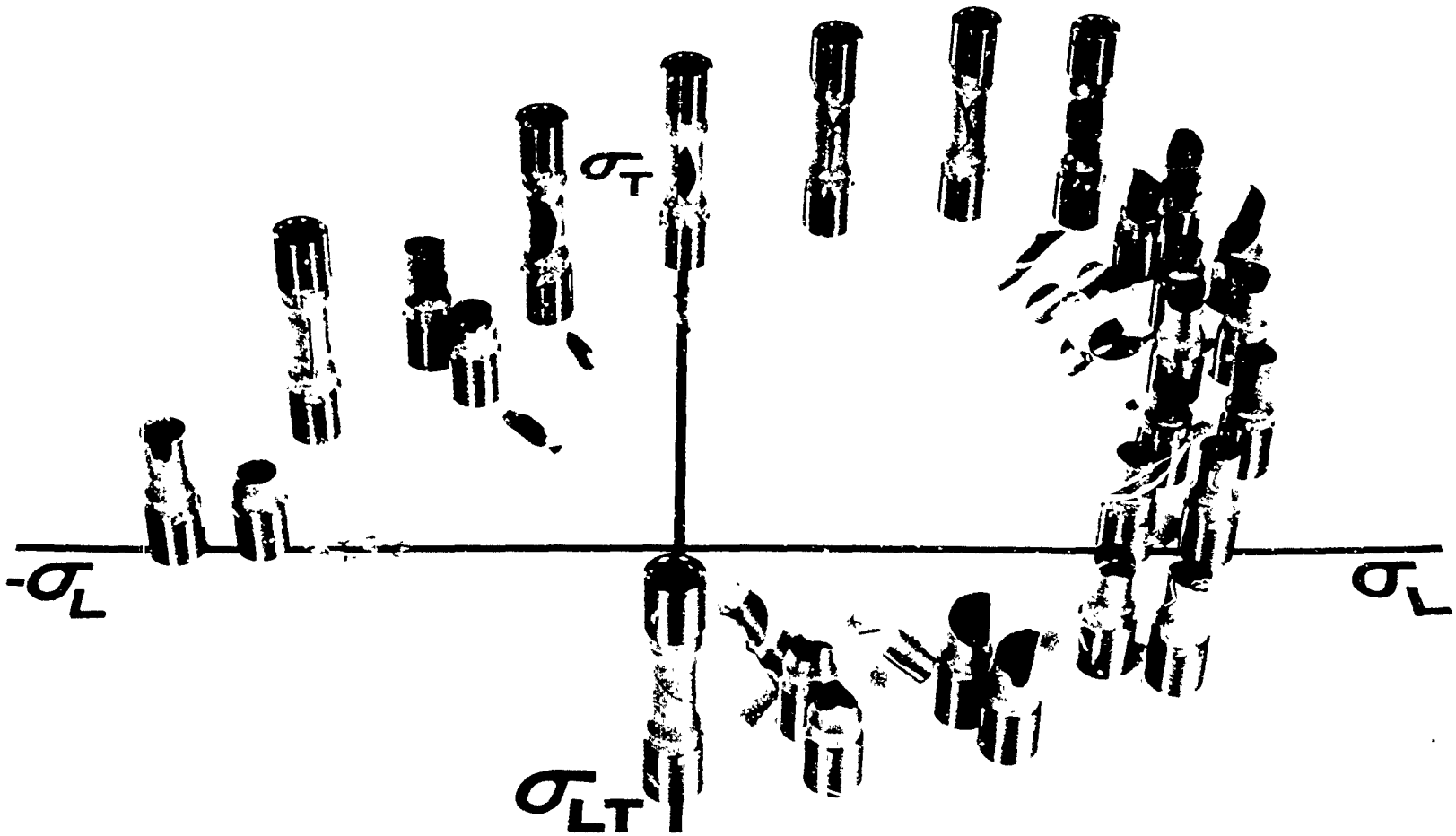

Figure 8. Failed Biaxial Specimens (XN50C)

The test results for the KBI P1 beryllium are given in Table II and in Figures 9 through 13.

Figures 9 and 10 present typical effective stress-strain curves. The P1 material has a higher yield strength and does not evidence the yield plateau exhibited by the Brush XN50C beryllium. Figure 9 shows the reversed loading curves for 2.5% compressive prestrain. These results are similar to Figure 3, showing the Baushinger effect for reloading in the reverse direction and increased yield strengths for subsequent loading in other directions. Figure 10 presents results for specimens prestrained in torsion to $\epsilon_{LT} = 2.5\%$. Again, these results are qualitatively comparable with Figure 5.

The biaxial strength loci are given in Figure 11. The 0.2% effective yield strength, $\bar{Y}_o$ has an average value of 42.0 ksi with a standard deviation of 1.82 ksi based upon 44 tests. The ultimate strengths are again compared with the Mogi criterion (Equations 4 and 5) with the constants

$$\sigma_t = 63 \text{ ksi}$$
$$\sigma_c = 79 \text{ ksi}$$
$$\sigma_{tt} = 63 \text{ ksi}$$

In the tension-tension quadrant the data again fall inside the Mogi locus, tending towards a constant maximum stress locus. Prestraining does not significantly raise or lower the stresses at failure.

The failure strains are plotted in Figure 12. Behavior is again similar in the two materials. Failure modes are illustrated in Figure 13. Because of the higher elastic strain energy stored in the P1 beryllium at failure, there is somewhat more fragmentation at failure and appearance of brittleness.

C. FRACTOGRAPHY

Scanning electron microscopy (SEM) was used to examine the features of typical fracture surfaces. Macroscopically, the Brush XN50C material has a higher ductility in all stress ratios than the KBI P1 material. However, the fracture surface topography, illustrated in the SEM fractographs of Figures 14 and 15, indicates much greater plastic flow associated with the fracture surface of the isostatically pressed KBI P1 beryllium (Figure 15). For all states of stress, the Brush XN50C hot pressed block specimens (Figure 14) exhibit transgranular brittle fracture facets of approximately grain size proportions. There is also evident a considerable amount of

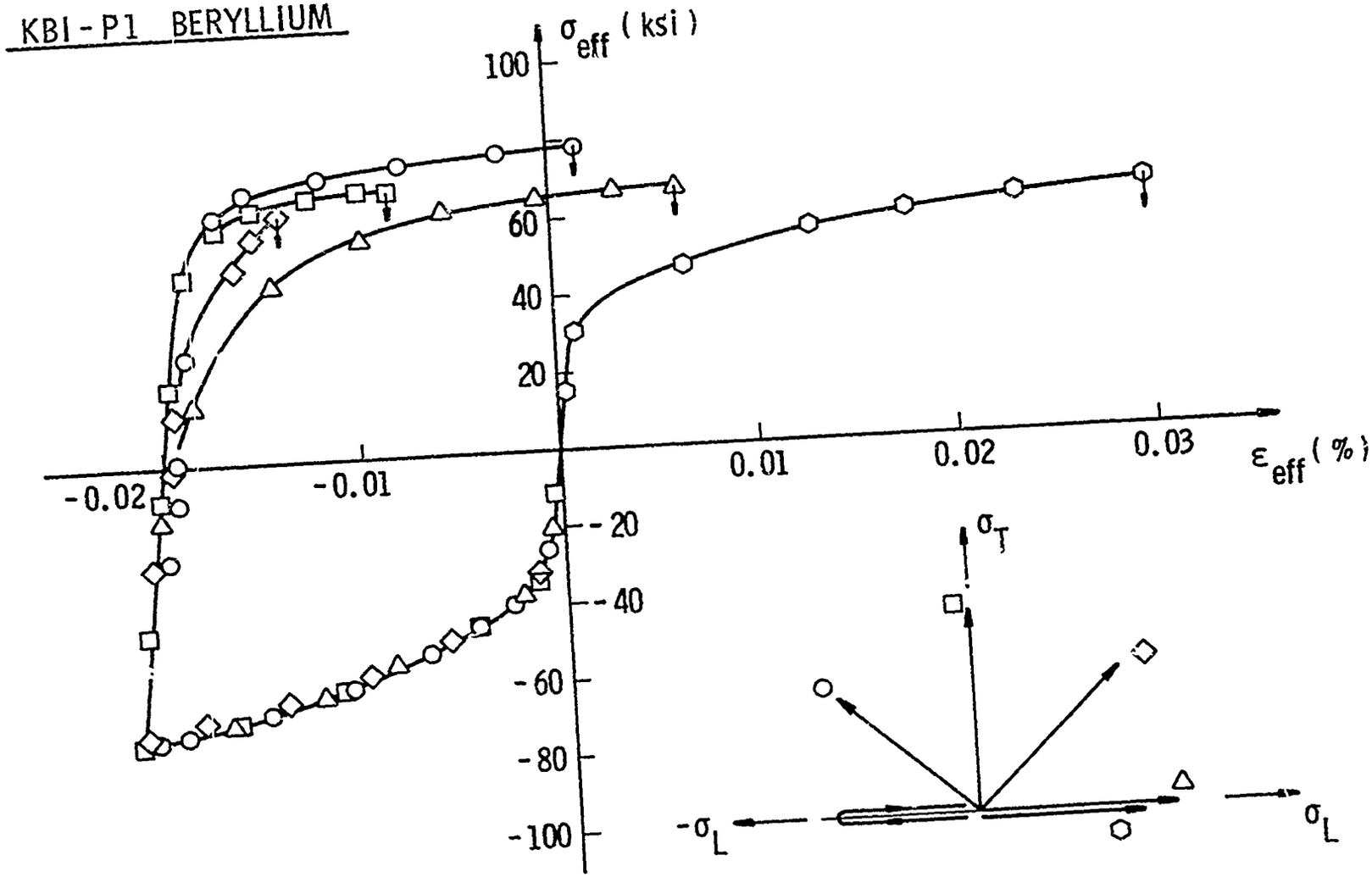

Figure 9. Effective Stress-Strain Curves for Be (P1), 2.5% Compressive Prestrain

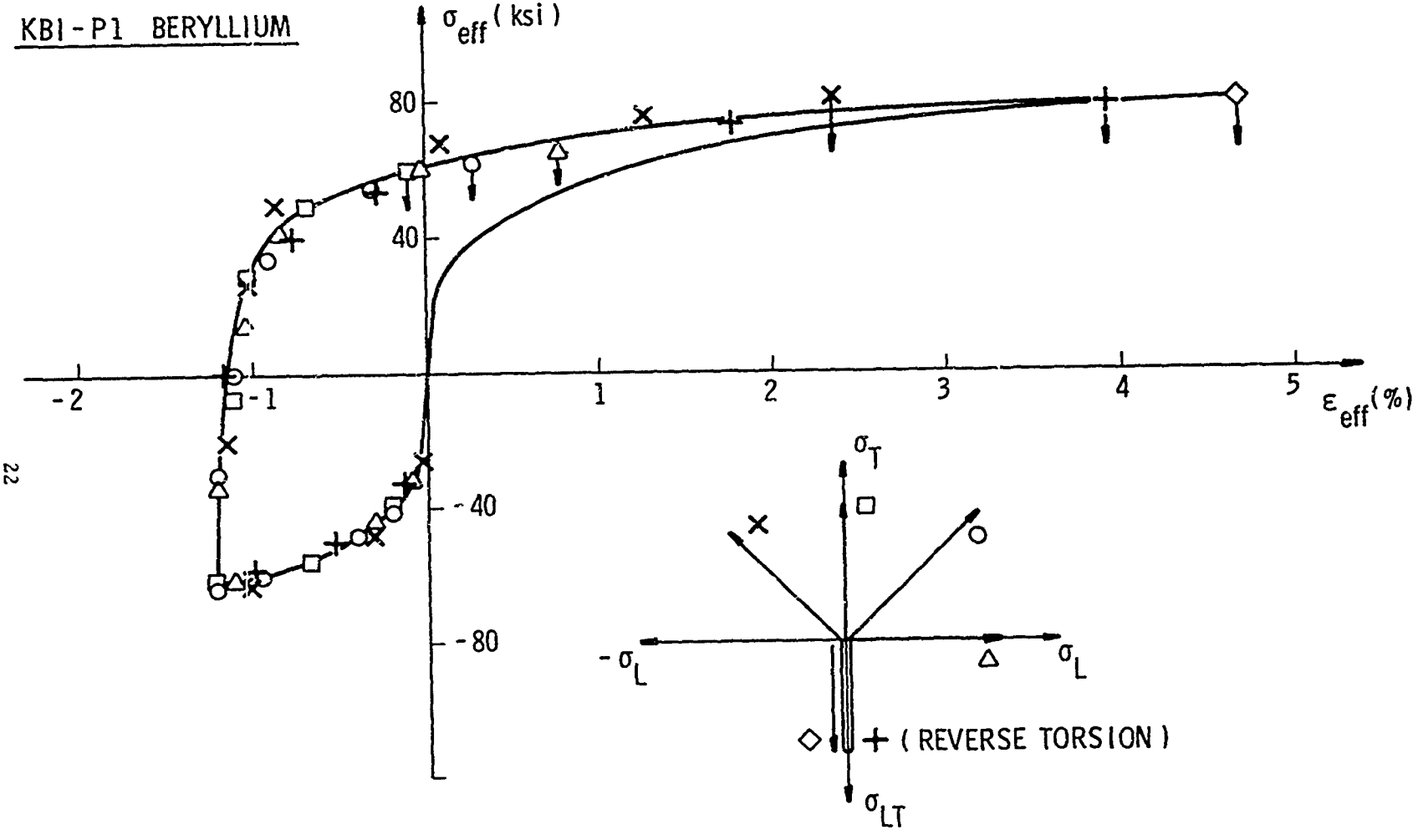

Figure 10. Effective Stress-Strain Curves for Be (P1), 2.5% Torsional Prestrain

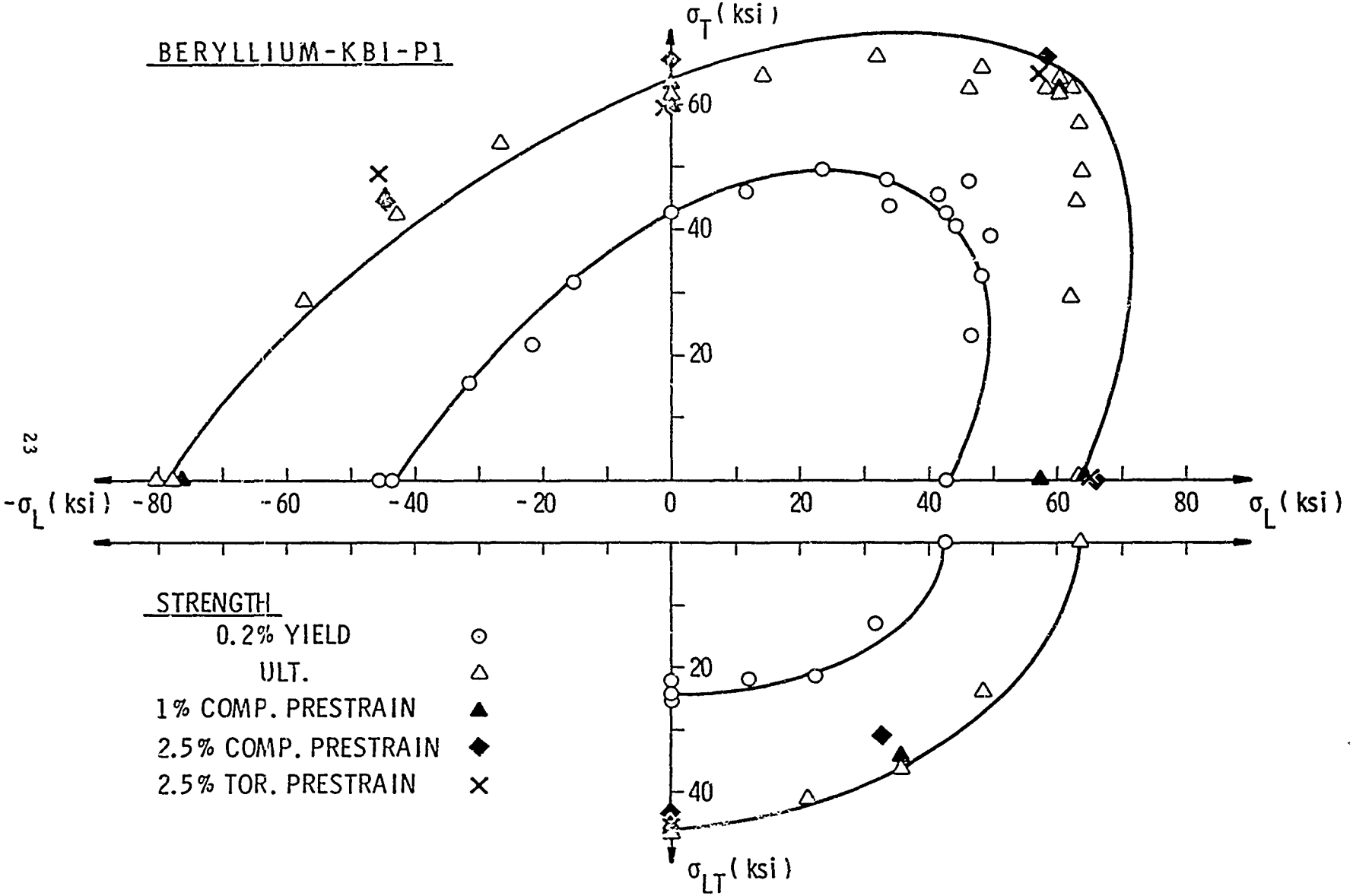

Figure 11. Biaxial Yield and Failure Strengths for Be (P1)

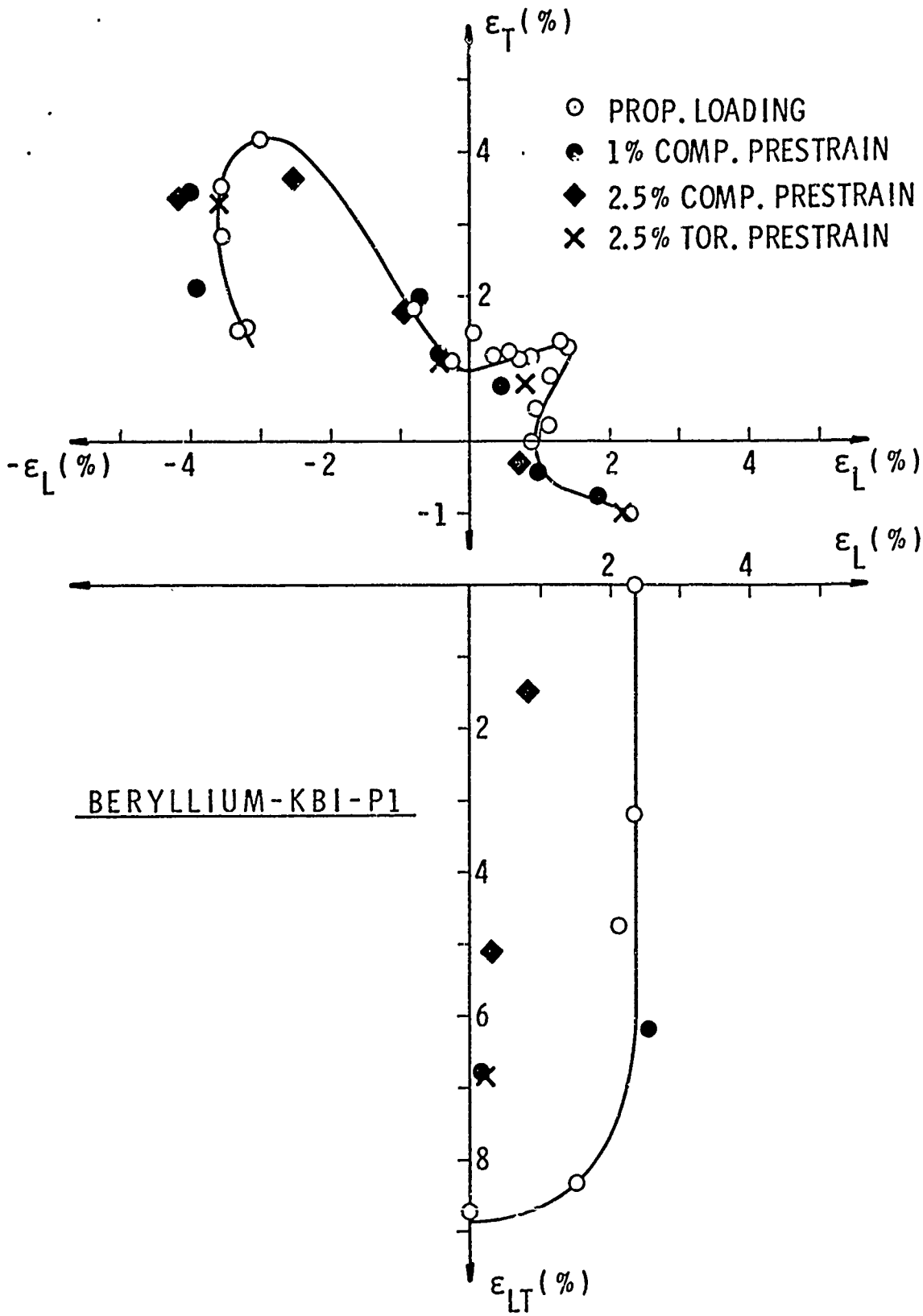

Figure 12. Biaxial Failure Strains for Be (P1)

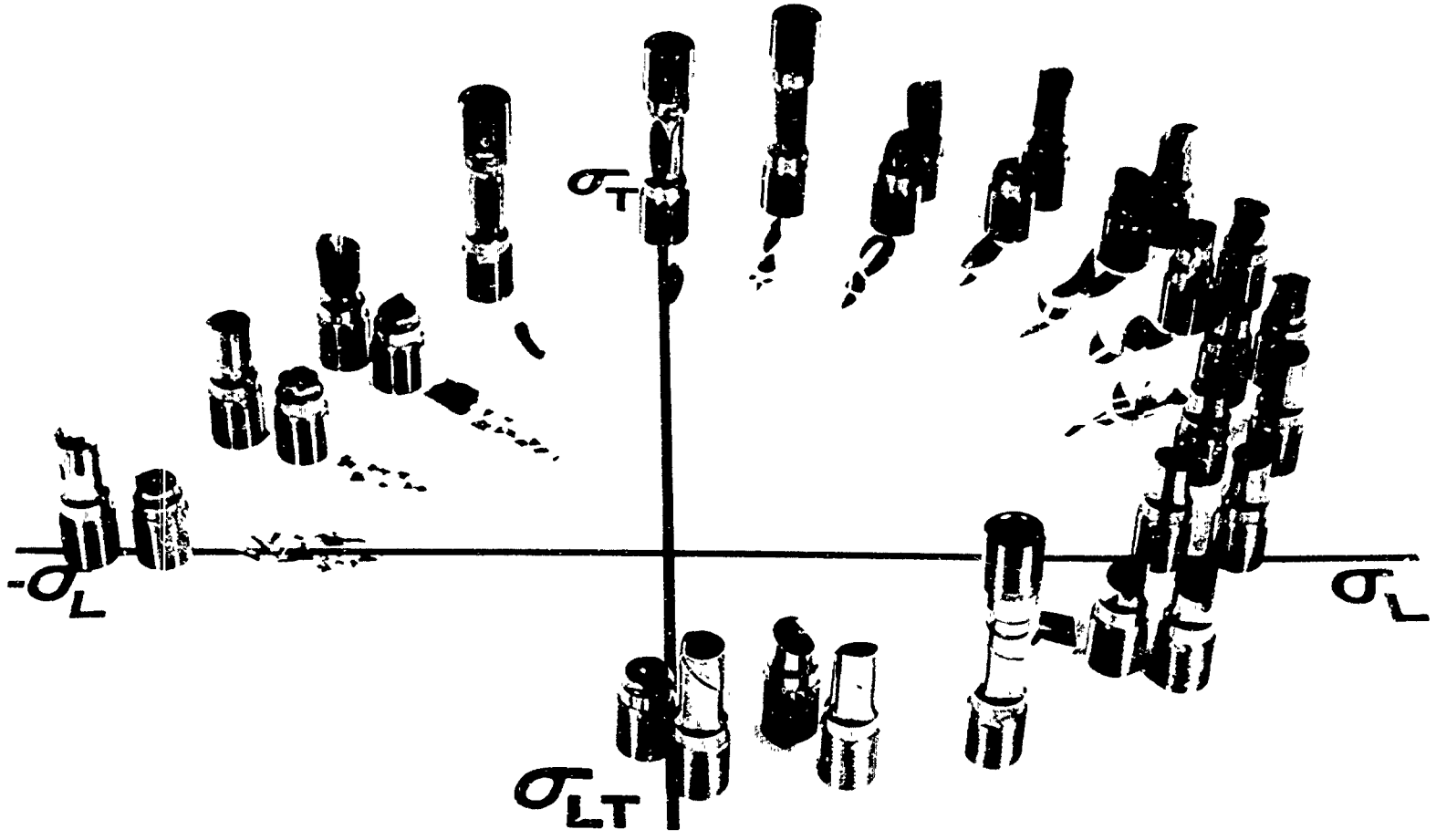

Figure 13. Failed Biaxial Specimens (P1)

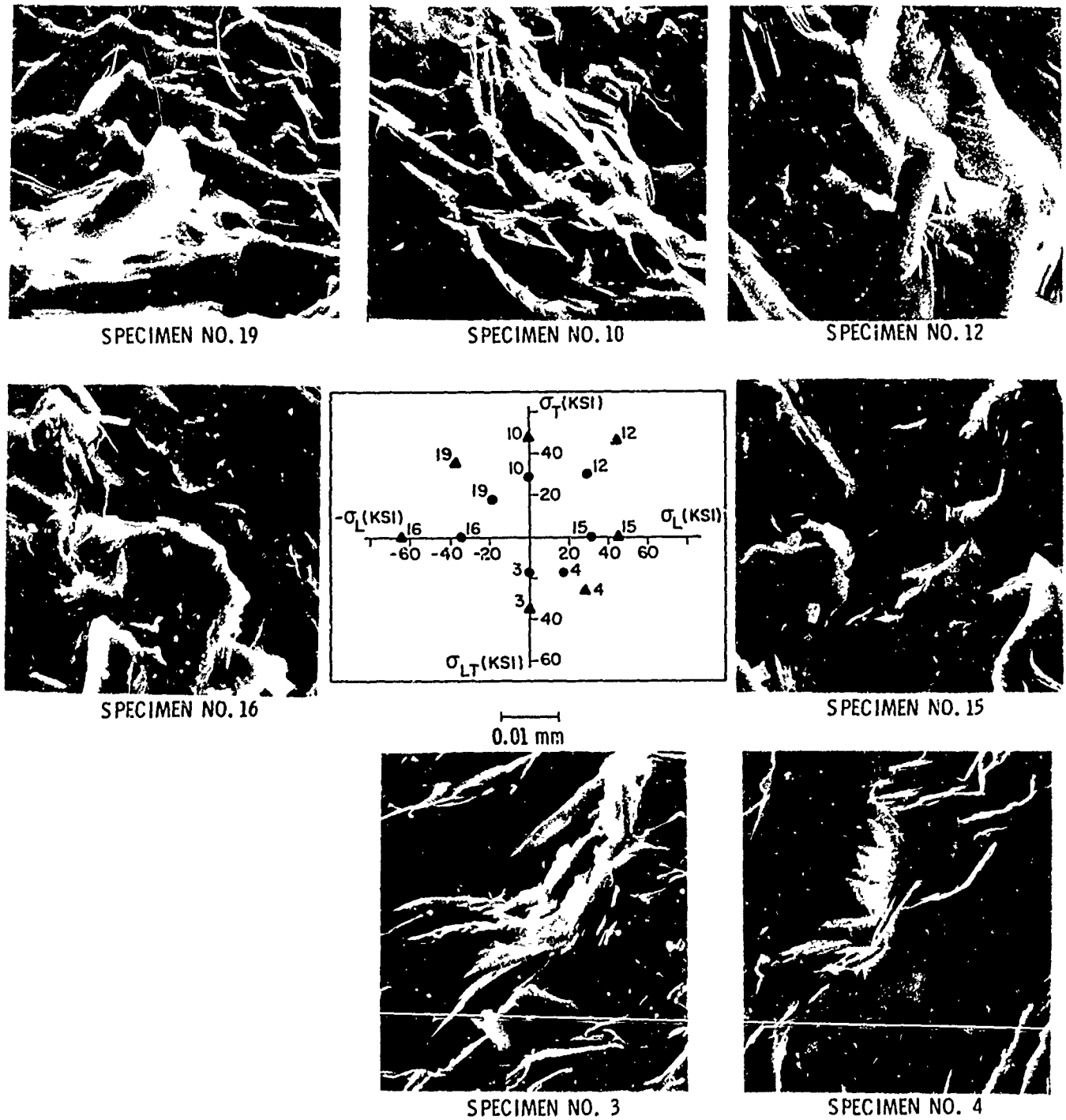

Figure 14. Effect of Stress Ratio on Fracture Surfaces of Be (XN50C)

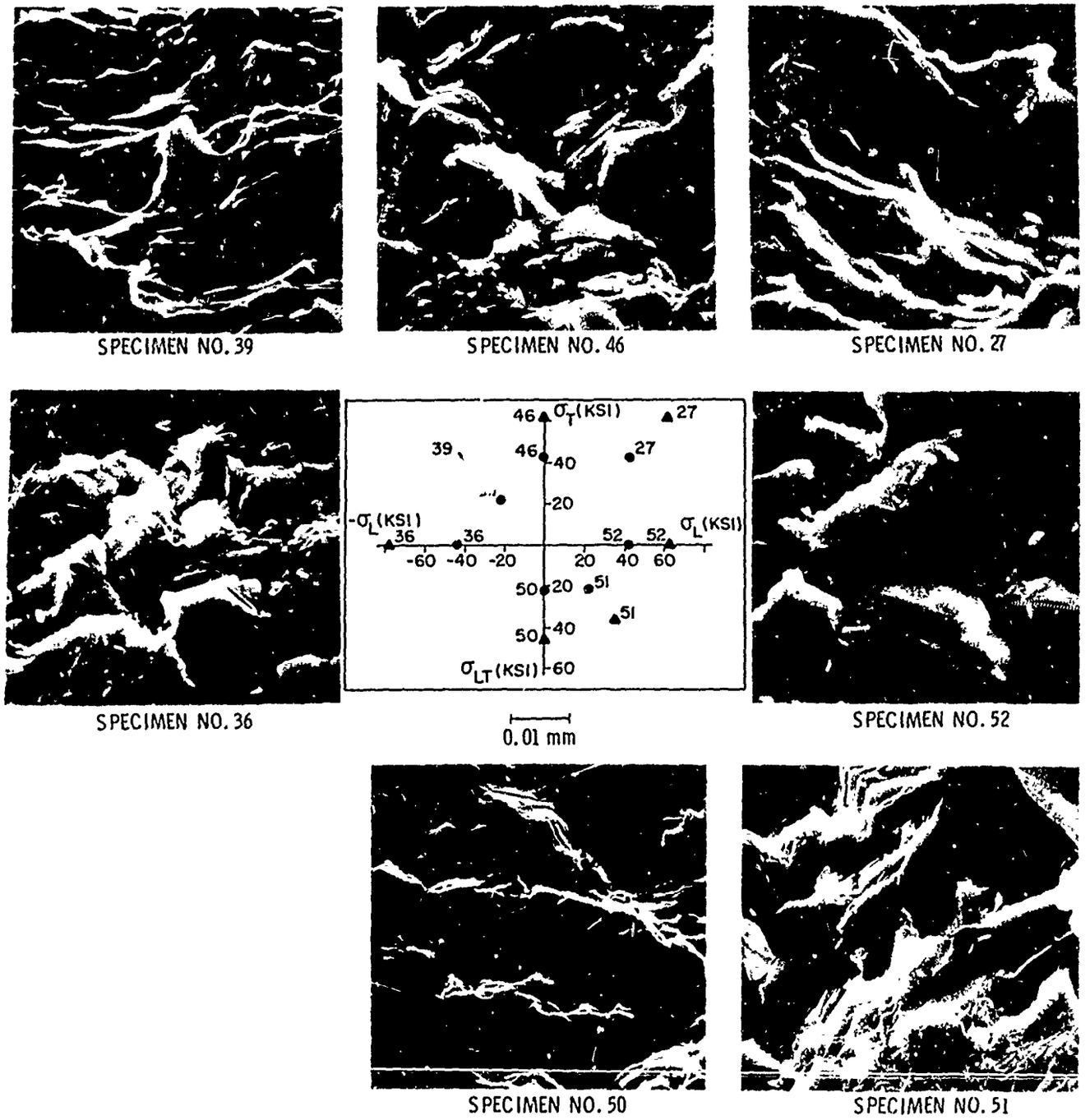

Figure 15. Effect of Stress Ratio on Fracture Surfaces of Be (P1)

secondary cracking, indicative of brittle behavior. On the other hand, the features of the KBI specimens (particularly numbers 52, 27 and 39) suggest fracture associated with considerable plastic flow. This plasticity is manifest by a less obviously transgranular mode of fracture, by a rounding of the numerous edges produced in the fracture process, and by the absence of secondary cracking.

There is also more variation in fracture topography with stress state in the KBI P1 material. Here again, curiously, the torsion specimen (No. 50) appears more brittle in fracture appearance than the biaxial tension specimen (No. 27). This is opposite to the ductility exhibited during the deformation process. These results suggest that the very localized plastic strain associated with creation of the fracture surface is not necessarily in proportion to the ductility determined from stress-strain behavior of bulk specimens.

Figure 16 shows a comparison between optical and SEM metallography. Figures 16A and 16B are SEM back scattered electron images of the polished and etched surfaces and fracture surfaces, respectively. Figure 16C shows the polished surface under polarized light to illustrate the grain structure. The grain size of the Brush material is larger and somewhat more uniform than the KBI P1. Grain size distribution is shown for both materials in Figure 17. Average grain size for KBI P1 is about 0.015 mm compared with 0.027 mm for the XN50C. In Figure 17A, the grain size distribution was measured directly from polished metallographic sections. In Figure 17B, the size of facets on the fracture surface was measured. The correspondence of the facet size with grain size shows that transgranular cleavage of single grains is the predominant fracture mode.

D. DISCUSSION

It is now possible to compare biaxial data for beryllium prepared as hot pressed block from three different powders, Brush's S-200E [Reference 1] and XN50C and KBI's HP-21 [Reference 3], and for KBI's P1 powder compacted by the CIP/HIP process. The strength and failure strain data are compared in Figures 18 and 19. Yielding in each case is isotropic, obeying a Mises yield criterion. Failure strengths are greater in compression than in tension, which can be accounted for by including a pressure dependent term in the failure criterion. This is physically consistent with the effect of pressure on crack nucleation and growth; compression retarding growth and tension accelerating growth. For beryllium, failure in the tension-tension quadrant appears to be limited by a maximum stress condition.

Biaxial ductility, as measured by strain at failure, is compared in Figure 19. Again, the data for each material show similar qualitative behavior. The reduction in ductility under biaxial tension and the shape of the curve in this quadrant will be discussed next.

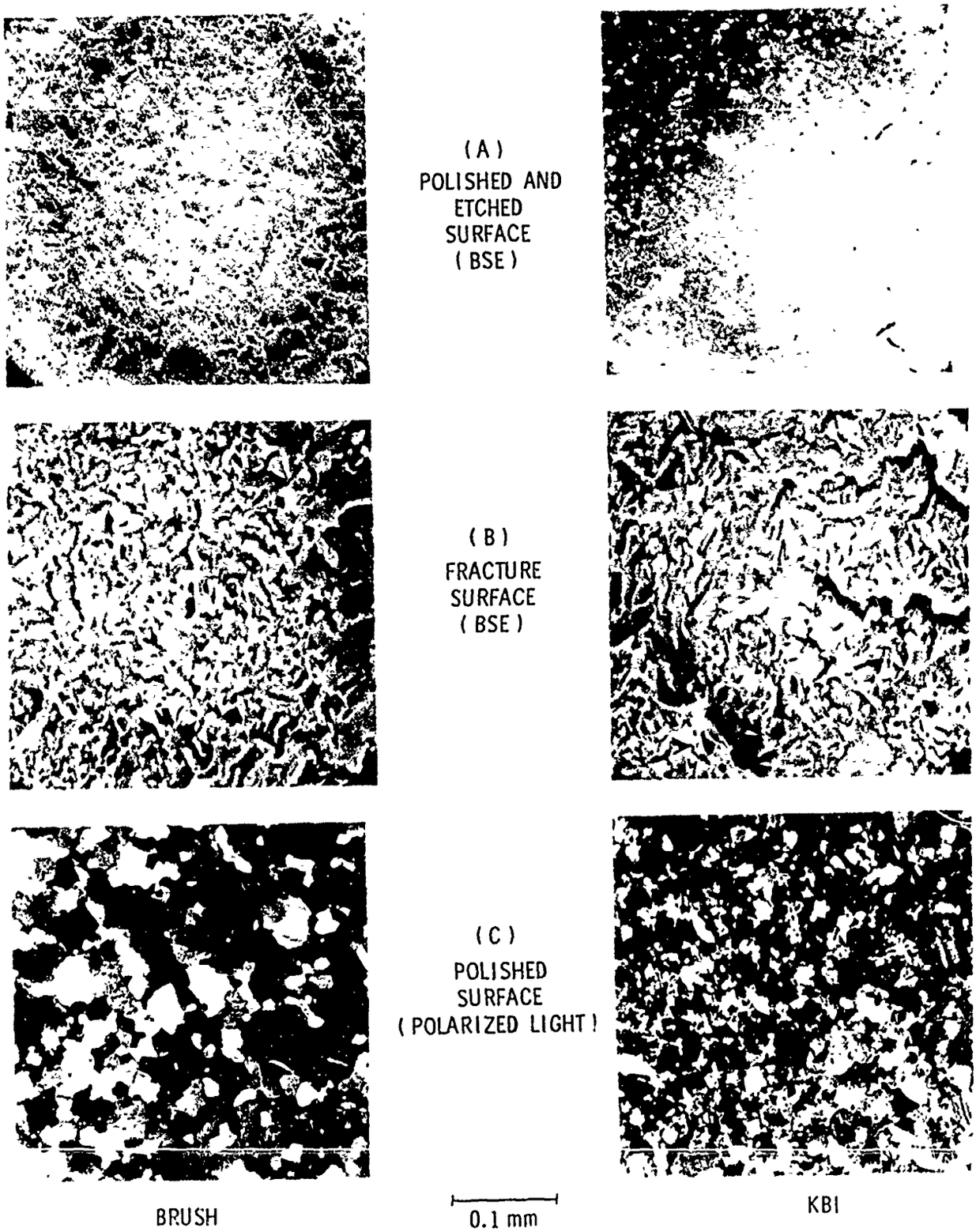

Figure 16. SLM. (A) and (B), and Optical (C) Metallography of Polished and Fracture Surfaces for Brush (XN50C) and KBI (PF) Beryllium. Note Relative Distribution of Pores (Dark) and Oxides (Light in (A).

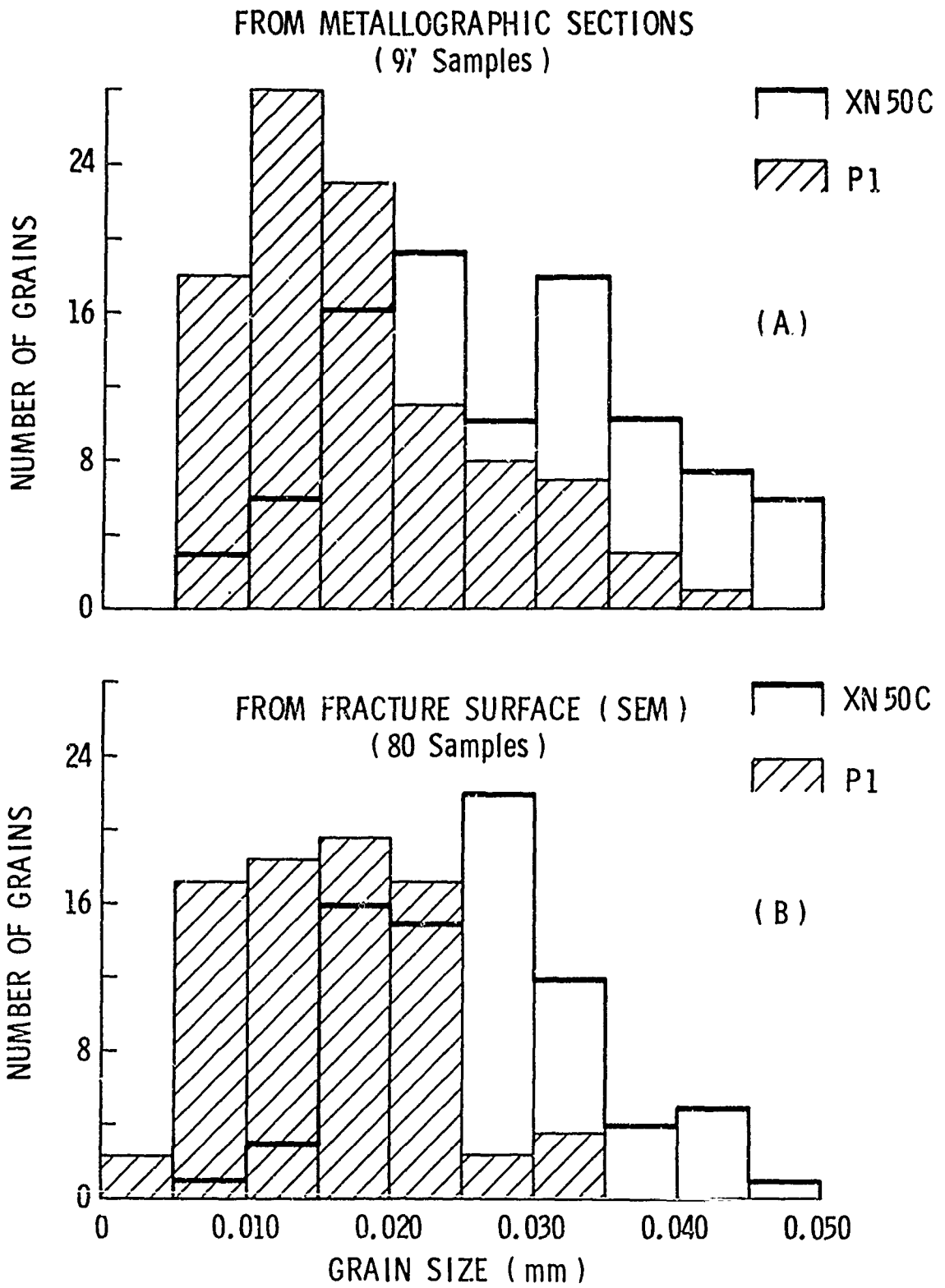

Figure 17. Comparison of Grain Size Distributions Obtained From Polished (A) and Fracture (B) Surfaces

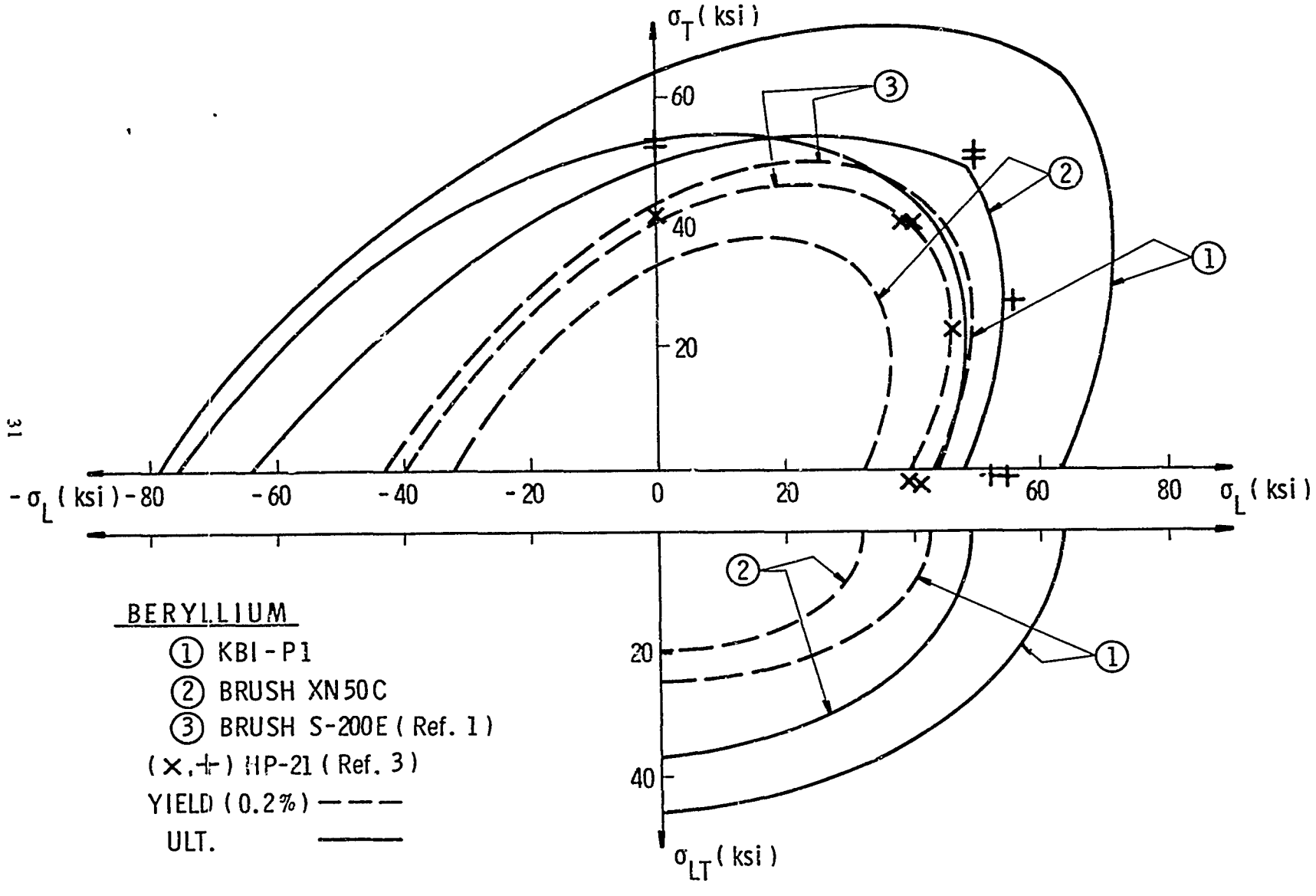

Figure 18. Comparison of Biaxial Strength for Four Types of Beryllium

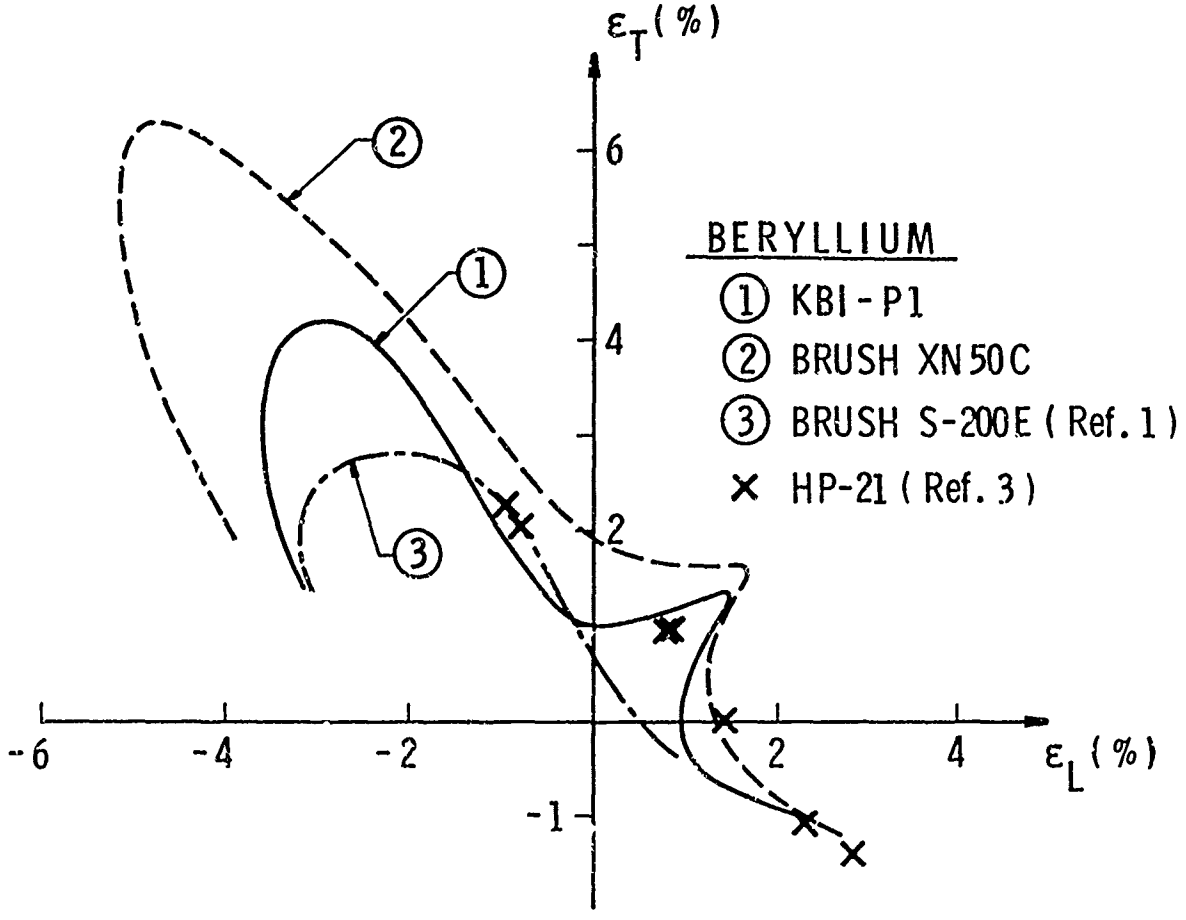

Figure 19. Comparison of Biaxial Failure Strains for Four Types of Beryllium

The shape of failure strain locus can be understood by comparing alternate failure criteria, as in Figure 20. The data points are for the KBI P1 material. For proportional loading paths we can assume the existence of an effective stress-strain relation

$$\sigma_{eff} = f(\epsilon_{eff}) \tag{7}$$

and the plasticity relations

$$\frac{\epsilon_L - \epsilon_T}{\sigma_L - \sigma_T} = \frac{2\epsilon_T + \epsilon_L}{\sigma_T} = \frac{2\epsilon_L - \epsilon_T}{\sigma_L} \tag{8}$$

where σ_{eff} and ϵ_{eff} are defined as in Equations 1 and 2 ($\sigma_{LT} = \epsilon_{LT} = 0$). Isotropy, small deformation and incompressibility are assumed. These two equations define the flow behavior, i.e., given the biaxial stress components, the strains are determined. Similarly, if the locus of failure stresses is specified the corresponding failure strains can be determined. Figure 20a shows three different stress failure criteria. The Mises criterion is

$$\sigma_{eff} = \bar{F}_o \tag{9}$$

where $\bar{F}_o$ is a constant. The Mogi criterion is given in Equation 5, and the Tresca or maximum shear stress criterion is

$$\left|\sigma_{max} - \sigma_{min}\right| = \bar{F}_o \tag{10}$$

It will be noted that all three criteria intersect on the stress axes and at equal biaxial tension.

Solving simultaneously Equations 7 and 8 with each stress failure criterion results in the failure strain loci shown in Figure 20b. The strain surface for the Mises criterion is ϵ_{eff} = constant, an ellipse rotated 90° with respect to the stress ellipse. For this condition, the distortional strain energy at failure would be constant for all stress ratios. For criterion where the stresses lie within the Mises ellipse, the strains will also be reduced in proportion to the stress difference and to the strain hardening modulus (from Equation 7).

The Tresca failure criterion agrees best with both the failure stress and strain experimental data and accurately describes the minima in failure strains at the intermediate stress ratios.

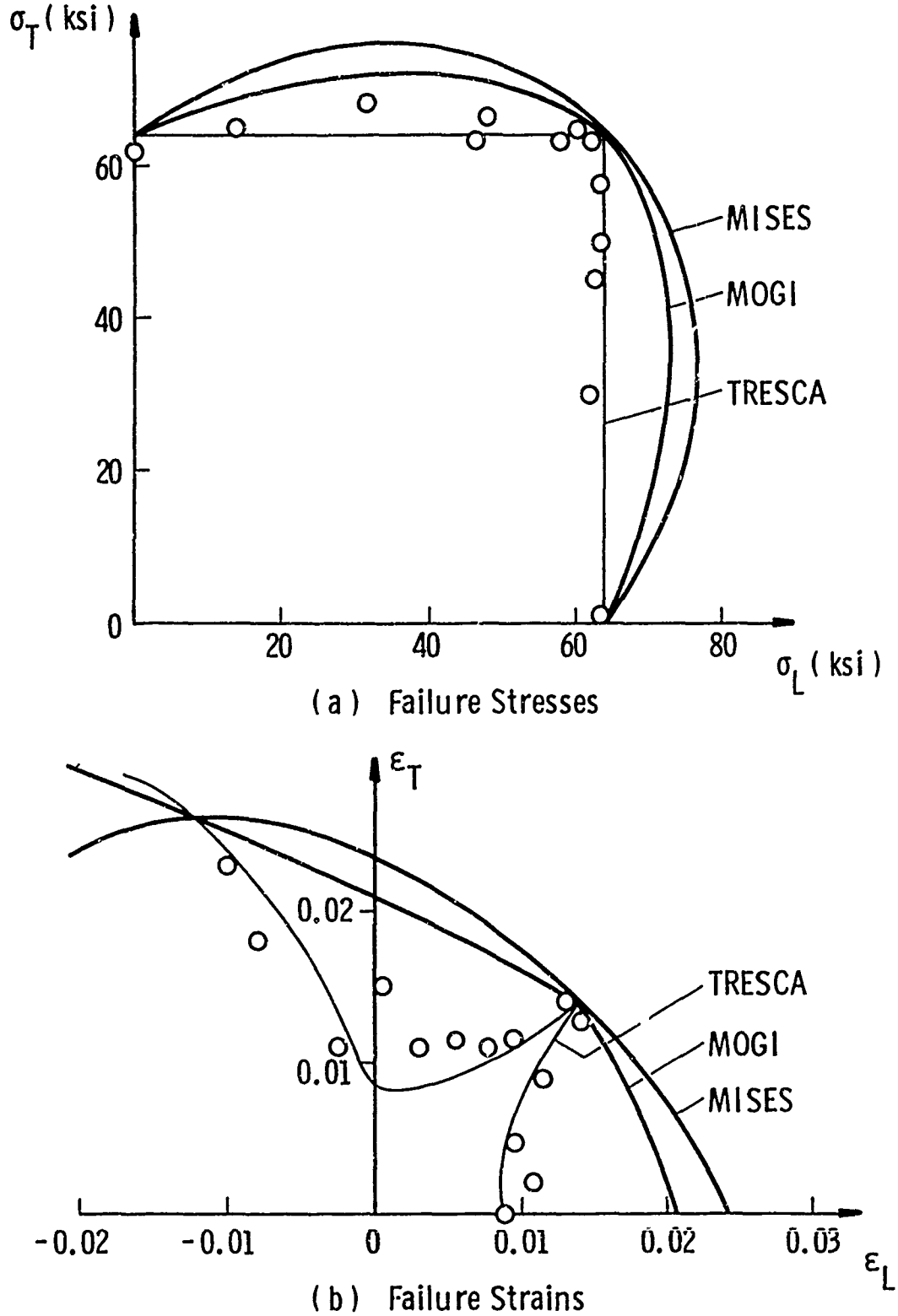

Figure 20. Comparison of Failure Stress and Strain Criteria With Experimental Data for Be (P1)

SECTION IV

TITANIUM

Two titanium alloys, 6Al-4V and 6Al-6V-2Sn, were tested to determine biaxial strength properties over the same range in stress states as the beryllium tests. The specimens were machined to the dimensions shown in Figure 2 from forged STA Centerless ground, 1.00-inch diameter titanium bar. Properties as certified by the supplier are given in Table III.

All tests were conducted to failure in proportional loading at an effective strain rate of 10^{-3} sec^{-1}. The titanium test data are summarized in Tables IV and V. Typical stress-strain curves for each alloy are given in Figure 21. Failure in compression and torsion was initiated by plastic buckling which may influence the ultimate stress values for these stress states. Because of buckling, failure strains are generally obtained only in the tensile quadrant.

Figures 22 and 23 are plots of the strength data. The stresses are plotted for both 0.02% and 0.2% offset yield strength and for the ultimate strength. There is a very narrow work hardening range for both alloys such that ultimate strength is very close to the 0.2% yield strength. A Mises ellipse is fit to the 0.2% yield values in each figure. For 6Al-4V, the average effective yield strength, $\bar{Y}_o$, is 162 ksi with a standard deviation of 8.17 ksi obtained from 10 tests. For 6Al-6V-2Sn, the average yield strength is 188 ksi with a standard deviation of 7.38 ksi obtained from 17 tests.

The failure stress is quite symmetric with the yield stresses. Any effect of the mean stress on ductile failure is not evident in this type of test.

Failure strains under biaxial tensile loading are given in Figure 24 for both alloys. The behavior is similar to the beryllium results, with perhaps a sharper minima in ductility at the stress ratios of 2:1. This is to be expected because of the very low (essentially zero) strain hardening modulus. These sharp variations in strain with stress ratio are accompanied by large variations in the total plastic work or energy required to rupture these alloys. This is illustrated in Figure 25. Near the uniaxial tensile or biaxial tensile axes, very small changes in stress ratio can result in an order of magnitude change in the energy to fracture. The practical significance of this is uncertain. Those processes, such as fatigue, which rely on the exhaustion of ductility could be influenced by this effect. It would be of

TABLE III. TITANIUM ALLOY PROPERTIES

Grade:	6Al-4V	6Al-6V-2Sn
1. Specification	AMS 4965A STA	MIL-T-9047D Type III, Comp. C
2. Chemistry (ingot)		
C %	0.02	0.02
N	0.010	0.008
Fe	0.18	0.78
Al	6.2	5.4
V	4.2	5.2
Sn		2.0
Cu		0.70
O	0.170	0.176
H (PPM Final Product)	98	53
3. Properties		
Ultimate (KSI)	171.7/170.1	187.0/229.8
Yield (KSI)	155.5/154.8	178.1/213.7
% Elongation	15.0/14.0	8.0/11.0
% R.A.	47.0/44.0	28.0/39.0
4. Thermal Treatment	Prod. STA 1750°F 1 hr, W.Q., Age 1000°F 4 hrs, Air Cooled	Prod. STA 1625°F 1 hr, W.Q., Age 1125°F 4 hrs, Air Cooled

TABLE IV. DATA SUMMARY - TITANIUM 6Al-4V

Specimen No.	0.02/0.2% Yield Strength (KSI)			Ult. Strength (KSI)			Strain at Fracture (%)		
	σ_L	σ_T	σ_{LT}	σ_L	σ_T	σ_{LT}	ϵ_L	ϵ_T	ϵ_{LT}
T- 30	120/151	0/0	0/0	170	0	0		No failure	
31	0/0	0/0	82/92	0	0	92.5		Buckling	
32	31/77	0/0	69/90	94.5	0	80.6		Buckling	
33	113/138	0/0	33.4/40.7	151	0	44.5		Buckling	
34	0/0	140/160	0/0	0	171	0	-4.1	17.0	--
35	144/164	150/170	0/0	180	187	0	3.1	3.8	--
36	150/177	75/88	0/0	202	100	0	9.65	- 0.65	--
37	92/103	184/205	0/0	107	214	0	0.25	1.7	--
38	-136/163	0/0	0/0	-172	0	0		Buckling	
39	- 31/96	80/95	0/0	-100	99	0	-1.6	1.35	--

TABLE V. DATA SUMMARY - TITANIUM 6Al-6V-2Sn

Specimen No.	0.02/0.2% Yield Strength (KSI)			Ult. Strength (KSI)			Strain at Fracture (%)		
	σ_L	σ_T	σ_{LT}	σ_L	σ_T	σ_{LT}	ϵ_L	ϵ_T	ϵ_{LT}
T- 26	--/184	0/0	0/0	187	0	0	10.0	-5.0 (est)	0.38
27	0/0	0/0	101/--	0	0	107		Buckling	
28	87/100	0/0	75/86	102	0	87.5	1.1	--	2.7
29	154/168	0/0	45/49	175	0	51.0		No failure	
40	-173/190	0/0	0/0	--	0	0		Buckling	
41	-102/112	102/112	0/0	-116	116	0	- 1.43	1.30	--
42	0/0	170/187	0/0	0	195	0	- 3.1	5.25	--
43	98/104	189/201	0/0	107	206	0	0.25	1.75	--
44	170/190	171/191	0/0	204	205	0	4.02	3.92	--
45	187/207	94/103	0/0	218	109	0	4.04	0	--
46	170/203	0/0	0/0	223	0	0		No failure	
47	180/202	44/48	0/0	211	52	0	5.47	1.36	--
48	180/198	137/150	0/0	209	159	0	2.55	0.65	--
49	141/156	196/217	0/0	166	232	0	0.25	1.70	--
50	46/55	184/220	0/0	60	241	0	- 0.20	1.90	--
51	176/186	176/186	0/0	198	198	0	3.83	4.52	--
52	62/80	176/227	0/0	85	240	0	- 0.12	1.74	--

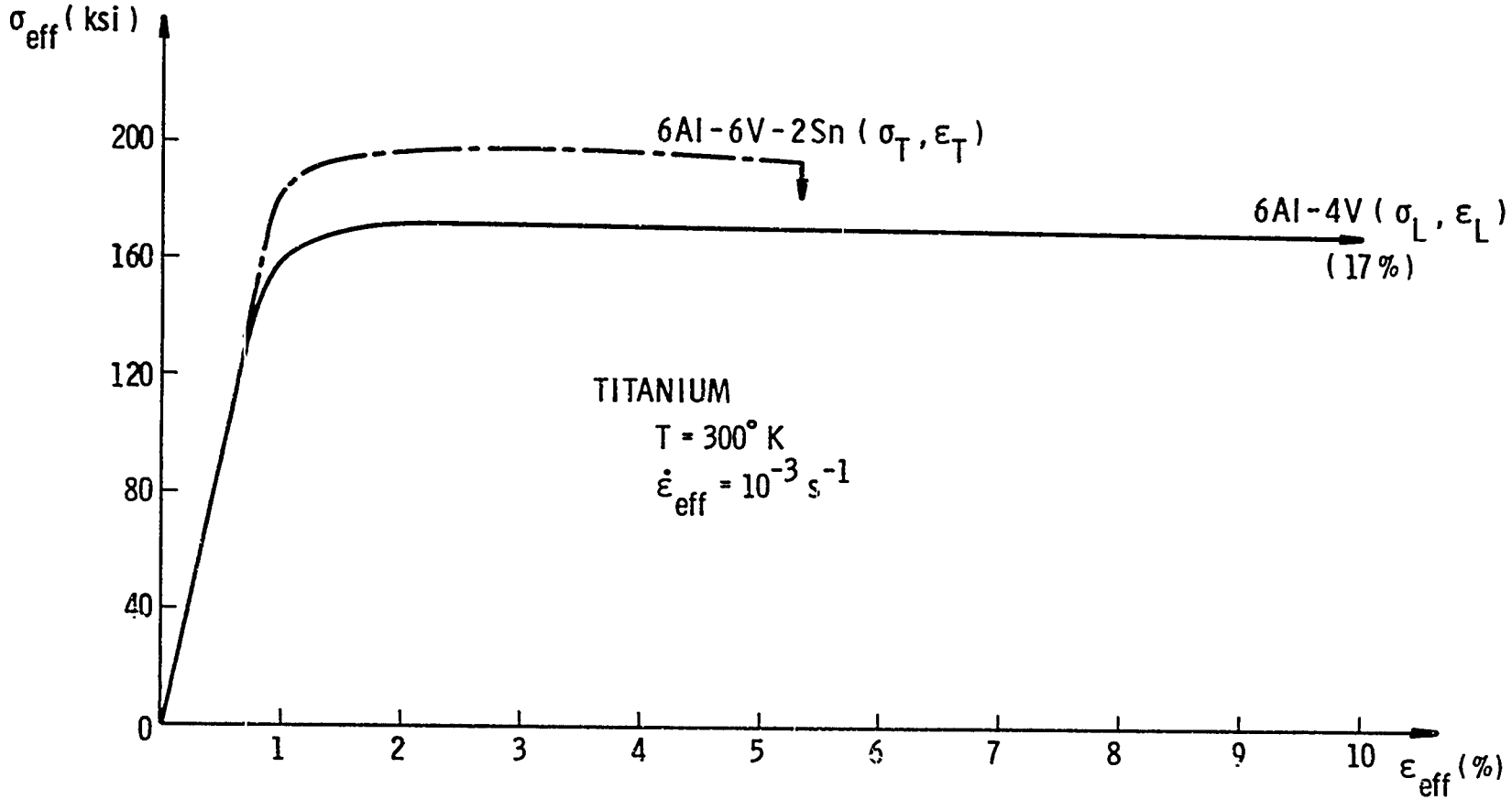

Figure 21. Stress-Strain Curves for Titanium 6Al-4V and 6Al-6V-2Sn

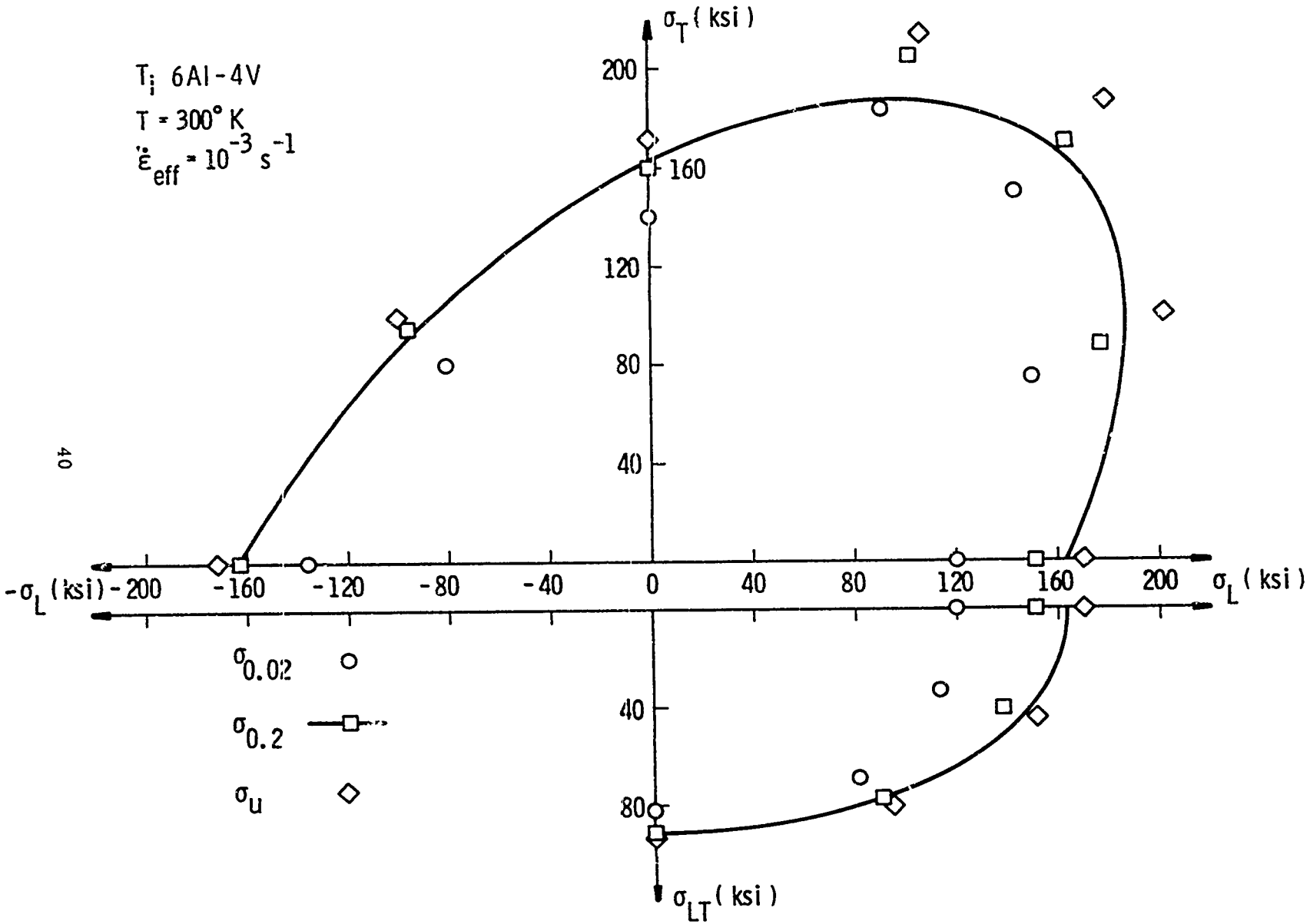

Figure 22. Biaxial Yield and Ultimate Strengths for Ti 6Al-4V

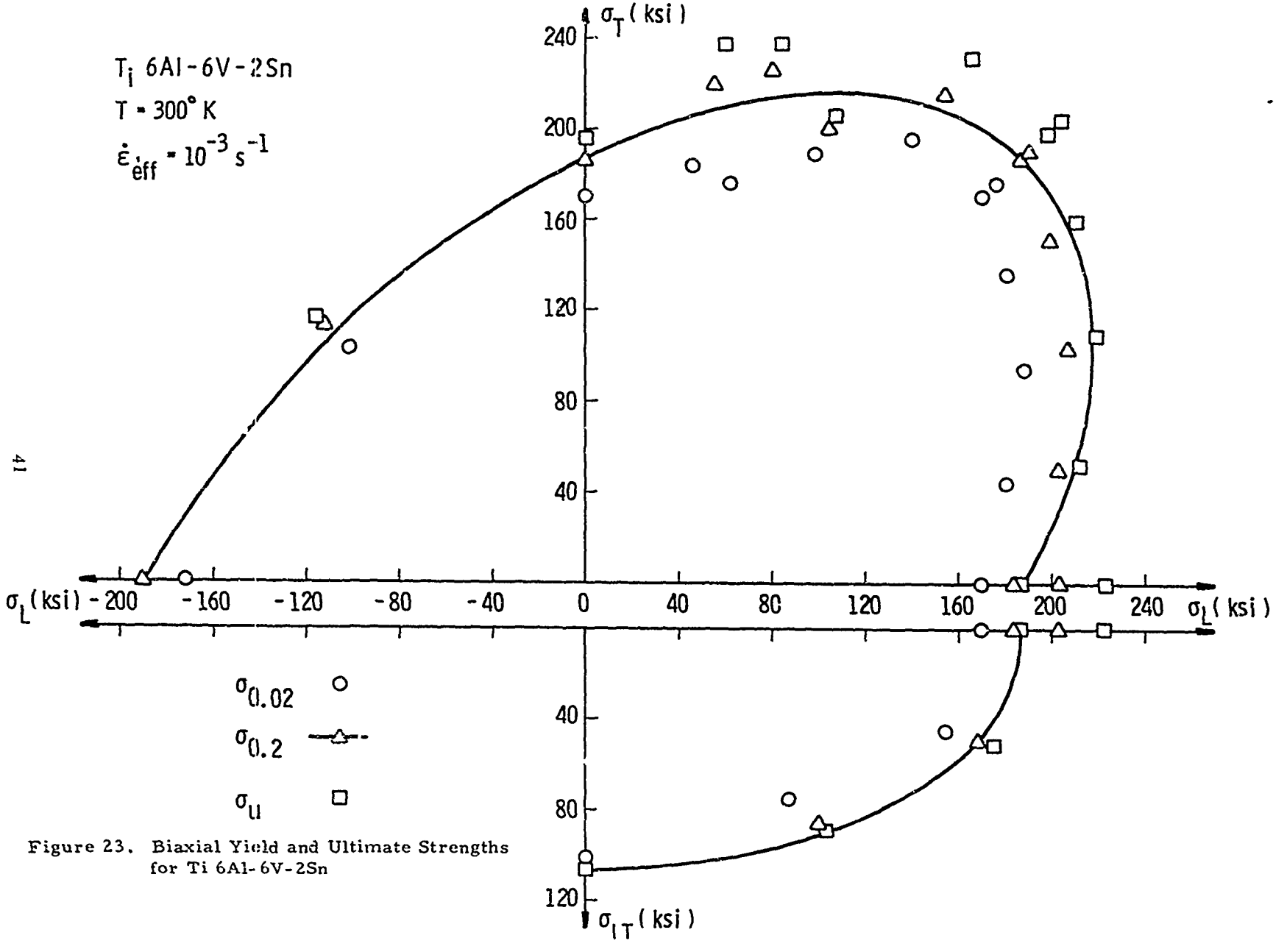

Figure 23. Biaxial Yield and Ultimate Strengths for Ti 6Al-6V-2Sn

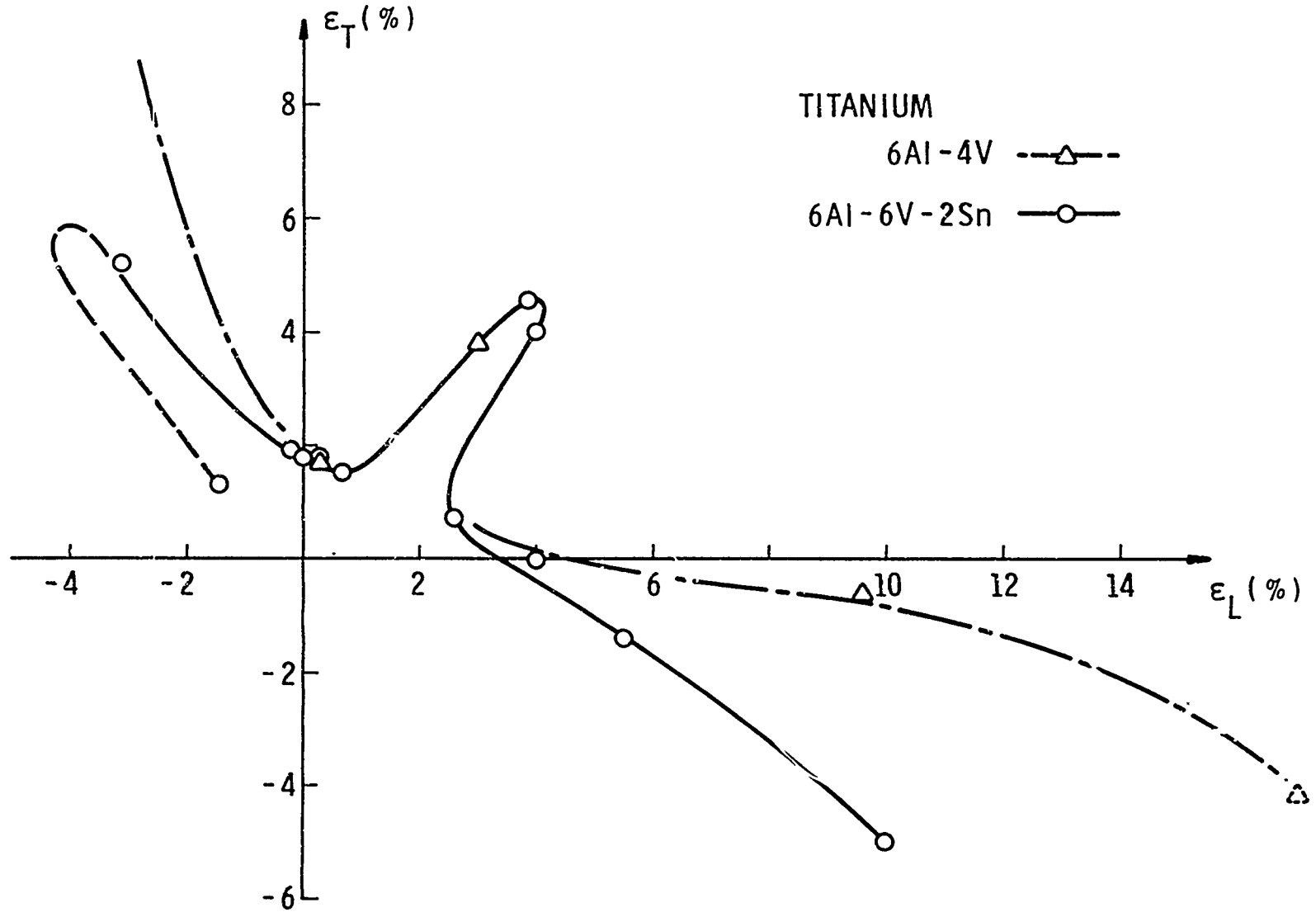

Figure 24. Biaxial Failure Strains for Ti 6Al-4V and 6Al-6V-2SN

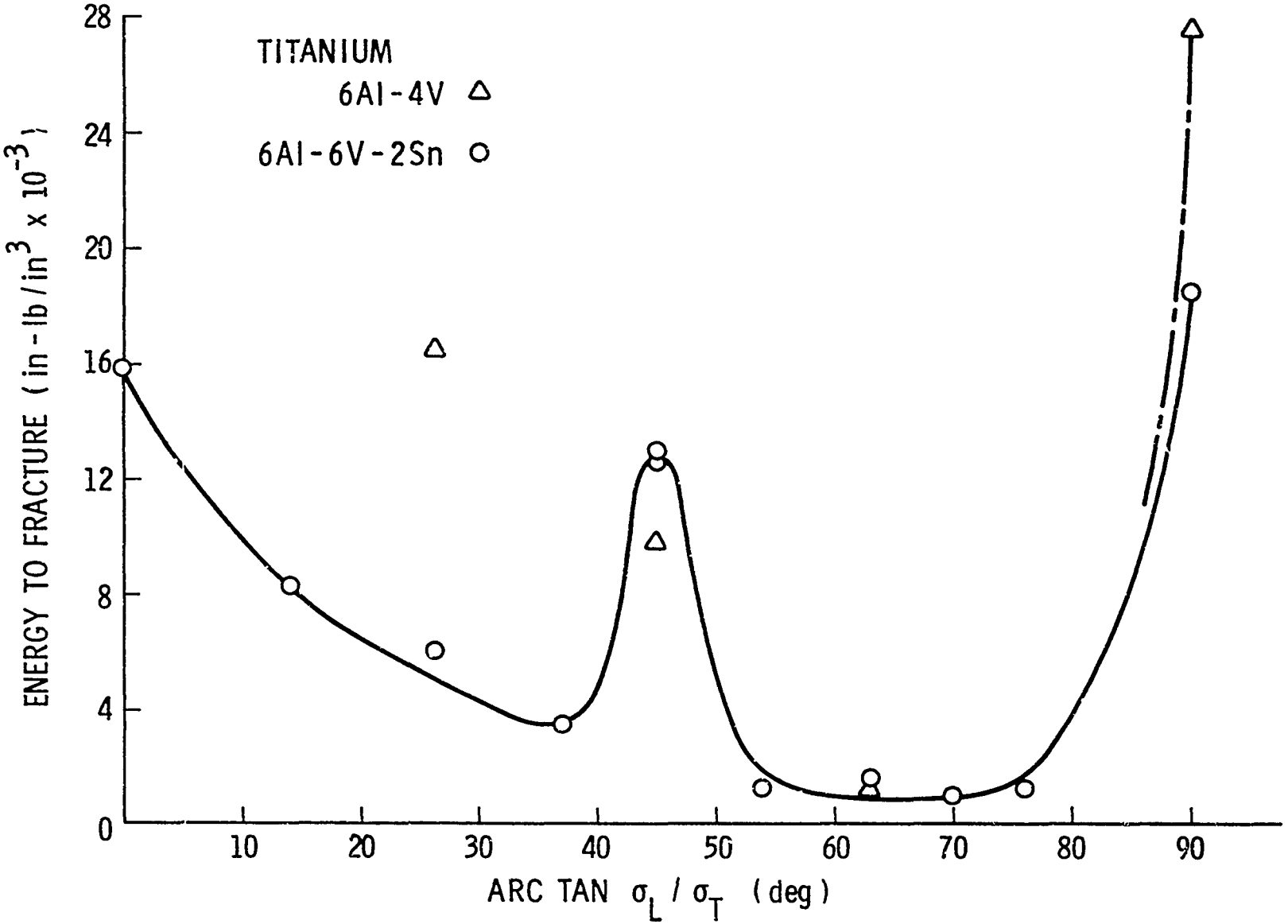

Figure 25. Effect of Stress Ratio on the Plastic Strain Energy Required to Produce Failure in Titanium

interest to examine biaxial fatigue life at these stress ratios. These results might also suggest that a spherical pressure vessel where the in-plane stress ratio is 1:1 will be much safer with respect to rupture than a closed-end cylindrical vessel where the ratio is 2:1.

SECTION V

CONCLUSIONS

The results presented for biaxial strength of beryllium and titanium can be summarized in the following general conclusions.

(1) The yield and plastic flow of both the beryllium and the titanium alloys tested can be described by a Mises yield criterion and associated flow rule for proportional loading.

(2) Failure stresses in beryllium are influenced by the mean or hydrostatic component of the stress. This effect is not evident in the more ductile titanium.

(3) In the critical tension-tension quadrant, failure strength of beryllium is best described by a maximum stress criterion.

(4) For both beryllium and titanium, there is significant variation in the biaxial ductility as measured by the total effective strain at failure. Minima in ductility occur at a ratio of the principal stresses of $\sigma_{max}:\sigma_{min} = 2:1$ in the tensile quadrant. The largest ductility is achieved in pure shear. Equal biaxial tension has ductility comparable with the uniaxial ductility. The behavior of the biaxial failure strains can be determined by combining the failure stress criterion with the appropriate plastic flow relations. This analysis shows that the range in biaxial ductility is strongly dependent on the plastic strain hardening modulus. Low strain hardening can lead to very low biaxial ductility as is demonstrated by the titanium data.

(5) Prestraining, or more generally a non-proportional loading history, has an effect on both the subsequent strain hardening curve and on the fracture strains in beryllium. Reversed loading in the same stress direction results in a reduced yield stress (Baushinger effect). Subsequent loading in other stress directions can produce yielding at stresses as great as the maximum strain hardened state of the initial prestraining. The beryllium thus shows evidence of both isotropic and kinematic hardening behavior. Ductility was not significantly decreased by prestraining. Reversed loading can, in fact, lead to an increase in total cumulative strain to failure. The amount of prestrain and the stress ratio both influence ductility.

(6) Plasticity, evidenced on the fracture surfaces of failed beryllium surfaces by means of SEM examination, did not correlate with the bulk plastic behavior associated with deformation. Material or stress state conditions yielding low macroscopic ductility displayed evidence of appreciable plastic deformation on the fracture surface. However, failure is generally associated with transgranular cleavage of single grains in both beryllium alloys.

REFERENCES

1. U. S. Lindholm and L. M. Yeakley, Effect of Strain Rate, Temperature and Multiaxial Stress on the Strength of S-200E Beryllium and 6Al-4V Titanium, AFML-TR-71-37, Wright-Patterson AFB, Ohio, March 1971.

2. U. S. Lindholm, L. M. Yeakley and A. Nagy, Development of a High Speed Biaxial Testing Machine, AFML-TR-71-149, Wright-Patterson AFB, Ohio, July 1971.

3. J. Jortner, "Behavior of Beryllium under Biaxial Stresses," presented at 1973 WESTEC Conf., Los Angeles, California, March 1973.

4. T. Nicholas and M. J. Sever, Reverse Loading Effects in Bend Tests on Hot Isostatically Pressed (HIP) Beryllium, AFML-TR-73-258, Wright-Patterson AFB, Ohio, March 1974.

5. K. Mogi, "Effect of the Triaxial Stress System on the Failure of Dolomite and Limestone," Tectonophysics, 11, 111, 1971.

U.S.Government Printing Office: 1974 — 657-015/238